© 2017. Published by The Company of Biologists Ltd | Development (2017) 144, 3706-3718 doi:10.1242/dev.150755

RESEARCH ARTICLE

Klf5 maintains the balance of primitive endoderm versus epiblast specification during mouse embryonic development by suppression of *Fgf4*

Takuya Azami[1,2], Tsuyoshi Waku[3], Ken Matsumoto[1], Hyojung Jeon[2], Masafumi Muratani[4], Akihiro Kawashima[2], Jun Yanagisawa[5,6], Ichiro Manabe[7], Ryozo Nagai[8], Tilo Kunath[9], Tomonori Nakamura[10,11], Kazuki Kurimoto[10,11], Mitinori Saitou[10,11,12,13], Satoru Takahashi[2,6,14] and Masatsugu Ema[1,15,*]

ABSTRACT

The inner cell mass of the mouse blastocyst gives rise to the pluripotent epiblast (EPI), which forms the embryo proper, and the primitive endoderm (PrE), which forms extra-embryonic yolk sac tissues. All inner cells coexpress lineage markers such as *Nanog* and *Gata6* at embryonic day (E) 3.25, and the EPI and PrE precursor cells eventually segregate to exclusively express *Nanog* and *Gata6*, respectively. Fibroblast growth factor (FGF)–extracellular signal-regulated kinase (ERK) signalling is involved in segregation of the EPI and PrE lineages; however, the mechanism involved in *Fgf4* regulation is poorly understood. Here, we identified *Klf5* as an upstream repressor of *Fgf4*. *Fgf4* was markedly upregulated in *Klf5* knockout (KO) embryos at E3.0, and was downregulated in embryos overexpressing *Klf5*. Furthermore, *Klf5* KO and overexpressing blastocysts showed skewed lineage specification phenotypes, similar to FGF4-treated preimplantation embryos and *Fgf4* KO embryos, respectively. Inhibitors of the FGF receptor (Fgfr) and ERK pathways reversed the skewed lineage specification of *Klf5* KO blastocysts. These data demonstrate that *Klf5* suppresses Fgf4-Fgfr-ERK signalling, thus preventing precocious activation of the PrE specification programme.

KEY WORDS: Inner cell mass, Primitive endoderm, Epiblast, *Fgf4*, *Klf5*, Mouse

INTRODUCTION

Mammalian preimplantation embryo development segregates into three fundamental cell lineages. The first lineage segregation event separates an epithelial cell layer called the trophectoderm (TE) on the surface of the embryo, which gives rise to trophoblast tissues of the placenta, and the inner cell mass (ICM), which gives rise to the embryo proper and extra-embryonic mesoderm. The second lineage segregation event further differentiates the ICM into epiblast (EPI) cells and the primitive endoderm (PrE). EPI cells generate most of the embryo proper and are a source of pluripotent embryonic stem cells (ESCs), whereas the PrE generates visceral and parietal endoderm tissues, and these become the visceral and parietal yolk sacs (Rossant and Tam, 2009). After compaction, inner cells generated in the first wave of cell division (8- to 16-cell stage) mainly contribute to EPI cells, whereas inner cells generated in the second wave (16- to 32-cell stage) are biased towards PrE cells (Morris et al., 2010). However, a previous study did not observe such predetermination in EPI and PrE specification (Yamanaka et al., 2010).

Single-cell analysis revealed that inner cells at embryonic day (E) 3.25 randomly coexpress EPI and PrE markers and eventually acquire either an EPI or a PrE identity (Guo et al., 2010; Kurimoto et al., 2006; Ohnishi et al., 2014). The mechanism involved in the emergence and specification of EPI and PrE precursor cells is not fully understood (Bedzhov and Zernicka-Goetz, 2015; Hermitte and Chazaud, 2014). The cell fate of EPI and PrE precursors is still plastic at E3.75 and is fully committed to EPI and PrE cells at ∼E4.0-4.25 (Grabarek et al., 2012; Nichols et al., 2009; Yamanaka et al., 2010).

Nanog and *Gata6* mRNAs are detectable as early as the 2-cell stage (Guo et al., 2010), and both Nanog and Gata6 proteins are coexpressed in all inner cells at E3.25 (∼32 cells) (Dietrich and Hiiragi, 2007; Plusa et al., 2008). Variability in the initial *Nanog* expression level shows no correlation with that of *Gata6* in individual inner cells at E3.25 (Ohnishi et al., 2014). As embryos develop, the salt-and-pepper distributions of *Nanog* and *Gata6* are evident in ICM cells until E3.5-4.0 (Chazaud et al., 2006; Plusa et al., 2008). The establishment of this salt-and-pepper distribution of *Nanog* and *Gata6* is poorly understood; however, fibroblast growth factor (FGF)–extracellular signal-regulated kinase (ERK)

[1]Department of Stem Cells and Human Disease Models, Research Center for Animal Life Science, Shiga University of Medical Science, Seta, Tsukinowa-cho, Otsu, Shiga 520-2192, Japan. [2]Department of Anatomy and Embryology, Faculty of Medicine, University of Tsukuba, 1-1-1 Tennoudai, Tsukuba, Ibaraki 305-8575, Japan. [3]Graduate School of Pharmaceutical Sciences, The University of Tokyo, Hongo, Bunkyo-ku, Tokyo 113-0033, Japan. [4]Department of Genome Biology, Faculty of Medicine, University of Tsukuba, 1-1-1 Tennodai, Tsukuba, Ibaraki 305-8575, Japan. [5]Graduate School of Life and Environmental Sciences, University of Tsukuba, 1-1-1 Tennodai, Tsukuba, Ibaraki 305-8577, Japan. [6]Center for Tsukuba Advanced Research Alliance, University of Tsukuba, 1-1-1 Tennodai, Tsukuba, Ibaraki 305-8577, Japan. [7]Department of Cardiovascular Medicine, The University of Tokyo Graduate School of Medicine, Bunkyo, Tokyo 113-8655, Japan. [8]Jichi Medical University, 3311-1 Yakushiji, Shimotsuke, Tochigi 329-0498, Japan. [9]MRC Centre for Regenerative Medicine, School of Biological Sciences, University of Edinburgh, 5 Little France Drive, Edinburgh EH16 4UU, UK. [10]Department of Anatomy and Cell Biology, Graduate School of Medicine, Kyoto University, Yoshida-Konoe-cho, Sakyo-ku, Kyoto 606-8501, Japan. [11]JST, ERATO, Yoshida-Konoe-cho, Sakyo-ku, Kyoto 606-8501, Japan. [12]Department of Reprogramming Science, Center for iPS Cell Research and Application, Kyoto University, 53 Kawahara-cho, Shogoin Yoshida, Sakyo-ku, Kyoto 606-8507, Japan. [13]Institute for Integrated Cell-Material Sciences, Kyoto University, Yoshida-Ushinomiya-cho, Sakyo-ku, Kyoto 606-8501, Japan. [14]International Institute for Integrative Sleep Medicine, Life Science Center, and Laboratory Animal Resource Center, University of Tsukuba, 1-1-1 Tennodai, Tsukuba, Ibaraki 305-8577, Japan. [15]PRESTO, Japan Science and Technology Agency, 4-1-8 Honcho Kawaguchi, Saitama 332-0012, Japan.

*Author for correspondence (mema@belle.shiga-med.ac.jp)

J.Y., 0000-0002-7196-7513; I.M., 0000-0001-9481-6673; T.K., 0000-0002-8805-7356; M.E., 0000-0003-0645-6183

Received 22 February 2017; Accepted 25 August 2017

Development (2017) 144, 3706-3718 doi:10.1242/dev.150755

signalling is postulated to play key roles (Chazaud et al., 2006; Kang et al., 2013; Krawchuk et al., 2013; Nichols et al., 2009; Ohnishi et al., 2014; Yamanaka et al., 2010). Fgf4-Fgfr-ERK signalling determines the balance of the EPI and PrE cell lineages: overactivation of FGF signalling caused by exogenous FGF4 converts all ICM cells to PrE cells (Yamanaka et al., 2010), whereas all ICM cells acquire EPI identity when FGF signalling is blocked by small chemical inhibitors of Fgfr and ERK (Nichols et al., 2009), by gene knockout (KO) of *Fgf4* (Kang et al., 2013; Krawchuk et al., 2013), and by KO of the expression of the adapter molecule *Grb2* (Chazaud et al., 2006). *Fgf4* KO embryos show normal *Nanog* and *Gata6* expression levels at E3.25; thus, the initial coexpression of *Nanog* and *Gata6* is independent of *Fgf4* (Kang et al., 2013; Krawchuk et al., 2013; Ohnishi et al., 2014). Subsequently, the segregation of EPI and PrE precursor cells is believed to be mediated by reciprocal repression between Nanog and Gata6 (Singh et al., 2007). In agreement with this model, the loss of Gata6 results in a complete shift into the EPI lineage, while there is no effect on the Nanog expression level at E3.0-3.25; thus, the initial expression of Nanog is independent of Gata6 at E3.0-3.25 (Bessonnard et al., 2014; Schrode et al., 2014). Importantly, single-cell analysis showed that bimodal *Fgf4* expression precedes asymmetric Nanog and Gata6 expression and is the first sign of the segregation of the EPI and PrE lineages (Guo et al., 2010; Ohnishi et al., 2014). Currently, what regulates *Fgf4* at this developmental stage is unknown (Artus and Chazaud, 2014; Chazaud and Yamanaka, 2016).

Klf5, a member of the Krüppel-like factor (Klf) family of transcription factors, functions in the maintenance of pluripotency and in somatic cell reprogramming (Takahashi and Yamanaka, 2006). Klf5 marks a naïve state of human pluripotent stem cells (Chan et al., 2013; Theunissen et al., 2014). Target gene inactivation of *Klf5* causes failure of TE and ICM development (Ema et al., 2008; Lin et al., 2010), but the molecular mechanism underlying Klf5-regulated ICM development is not well understood.

Here, we show that the inner cells of *Klf5* KO embryos adopt a PrE lineage fate at the expense of EPI cells, while *Klf5*-overexpressing (OE) embryos show incomplete lineage segregation as indicated by the persistence of $Nanog^+/Gata6^+$ double-positive cells. We show that *Fgf4* expression is upregulated in *Klf5* KO embryos at E3.0, whereas *Fgf4* is repressed in *Klf5* OE blastocysts. Importantly, single-cell analysis clearly demonstrates that *Fgf4* is derepressed in a subset of *Fgf4*-high inner cells of *Klf5* KO embryos. Chromatin immunoprecipitation (ChIP) assays indicate that the *Fgf4* locus is occupied by Klf5, suggesting direct regulation of *Fgf4* by Klf5. In terms of the emergence of $Nanog^+$ pluripotent EPI cells, the phenotypes of *Klf5* KO embryos can be reversed by either Fgfr or ERK inhibition. Taken together, these results provide new insights into the interplay between *Klf5* and the Fgf4-Fgfr-ERK pathway crucial for the proper lineage segregation.

RESULTS

Skewed EPI and PrE lineage specification in *Klf5* KO and OE blastocysts

Although *Klf5* is indispensable for blastocyst development, the mechanistic functions of *Klf5* in ICM development and early lineage segregation remain elusive (Ema et al., 2008; Lin et al., 2010). In a previous study, the *Klf5-lacZ* allele (Ema et al., 2008) was generated by inserting a *lacZ* cassette into the second exon of *Klf5*, leaving the rest of the *Klf5* locus with the potential to generate a C-terminally truncated protein of ∼164 amino acids in length (Fig. S1A). To delete almost the entire open reading frame of *Klf5*, we generated a new KO mouse for *Klf5* that removes the two major coding exons (designated *Klf5*Δ2nd3rd exon) (Fig. S1B). Similar to *Klf5-lacZ* mice (Fig. S1A) (Ema et al., 2008), no homozygous pups were obtained from heterozygous intercrosses of the *Klf5*Δ2nd3rd exon mice, and homozygous $Klf5^{\Delta 2nd3rd\ exon/\Delta 2nd3rd\ exon}$ embryos showed implantation defects (Fig. S1C). When *Klf5* KO morulae ($Klf5^{lacZ/lacZ}$ or $Klf5^{\Delta 2nd3rd\ exon/\Delta 2nd3rd\ exon}$) at E2.5 were stained with antibodies against lineage markers such as Oct3/4 (Pou5f1) and Cdx2, both types of *Klf5* KO embryos showed decreased levels of Cdx2 and normal levels of Oct3/4 protein expression (Fig. S1D,E). Hereafter, the *Klf5*Δ2nd3rd exon allele was used as the null allele for our study.

To obtain insight into the role of *Klf5* in early embryogenesis, we established a new ESC line with Cre-mediated overexpression of the FLAG/HA-Klf5 cassette (Fig. S1F). We used the ESC line, which expresses GFP prior to Cre-mediated excision, to generate the conditional *Klf5* OE mice (Fig. S1G). Upon crossing to the Ayu1-Cre driver line, we confirmed that Klf5 protein is overexpressed 1.5-fold in *Klf5* OE blastocysts compared with wild type (WT) (Fig. S1H).

First, we collected embryos carefully timed every 6 h from E3.25 onwards and found that *Klf5* KO embryos had fewer cells than their WT counterparts (Fig. S1I). The total cell number per *Klf5* KO embryo never exceeded 64 until E4.25 (Fig. S1I; data not shown). Given that bromodeoxyuridine (BrdU) incorporation was severely affected, it is likely that cell cycle progression had been disturbed (Fig. S1J,K). Co-staining embryos from E3.25 to E3.5 for BrdU incorporation and terminal deoxynucleotidyl transferase-mediated dUTP nick-end labelling (TUNEL) showed that the cells defective in BrdU incorporation were $TUNEL^+$, suggesting that defective cell cycle progression was promoting apoptosis (Fig. S1L).

Examination of Nanog and Gata6 expression levels in *Klf5* KO embryos revealed that the initial Nanog and Gata6 expression at E3.25 was, overall, similar to that of WT embryos (Fig. 1A). Analyses of *Klf5* KO blastocysts at E3.5 and E3.75 showed that most, if not all, ICM cells were $Gata6^+$ and that few cells were $Nanog^+$ (Fig. 1A,C, Fig. S2A,C). Consistent with this result, Nanog protein expression levels decreased in *Klf5* KO embryos during development from E3.25 to E4.0, whereas Gata6 protein levels increased (Fig. 1B). Since it was reported that $Nanog^+/Gata6^+$ double-positive (DP) common precursors differentiate progressively into a $Nanog^+/Gata6^-$ ($Nanog^+$) EPI or $Nanog^-/Gata6^+$ ($Gata6^+$) PrE fate in an asynchronous manner (Saiz et al., 2016), we evaluated the percentage of DP cells, $Nanog^+$ cells and $Gata6^+$ cells from E3.25 to E4.0. The percentage of DP cells in *Klf5* KO embryos decreased rapidly and, in turn, the percentage of $Gata6^+$ cells increased, indicating that bipotential DP cells in *Klf5* KO embryos prefer to differentiate into $Gata6^+$ PrE cells (Fig. 1C). At the E4.0 late blastocyst stage, most cells in *Klf5* KO embryos acquired the $Gata6^+$ PrE fate (Fig. 1A,C).

Our finding that only Gata6-expressing cells in *Klf5* KO embryos remain at E4.0 could be the consequence of apoptosis of $Nanog^+$ EPI cells rather than of more cells differentiating into PrE. To gain insight into the role of apoptosis in the EPI lineage, we analysed the number of $TUNEL^+$ cells in *Klf5* KO and WT embryos at E3.5. We found no significant changes in the percentage of $Nanog^+$, $Gata6^+$, DP, or double-negative (DN) cells undergoing apoptosis between WT and *Klf5* KO embryos (Fig. S1M-O). This indicated that the increase in the percentage of $Gata6^+$ cells was not caused by the death of any specific cell lineage, including EPI cells. Because the percentage of DP cells in *Klf5* KO embryos was decreased (Fig. 1C), DP cells were likely to have differentiated into PrE. Because the

Development (2017) 144, 3706-3718 doi:10.1242/dev.150755

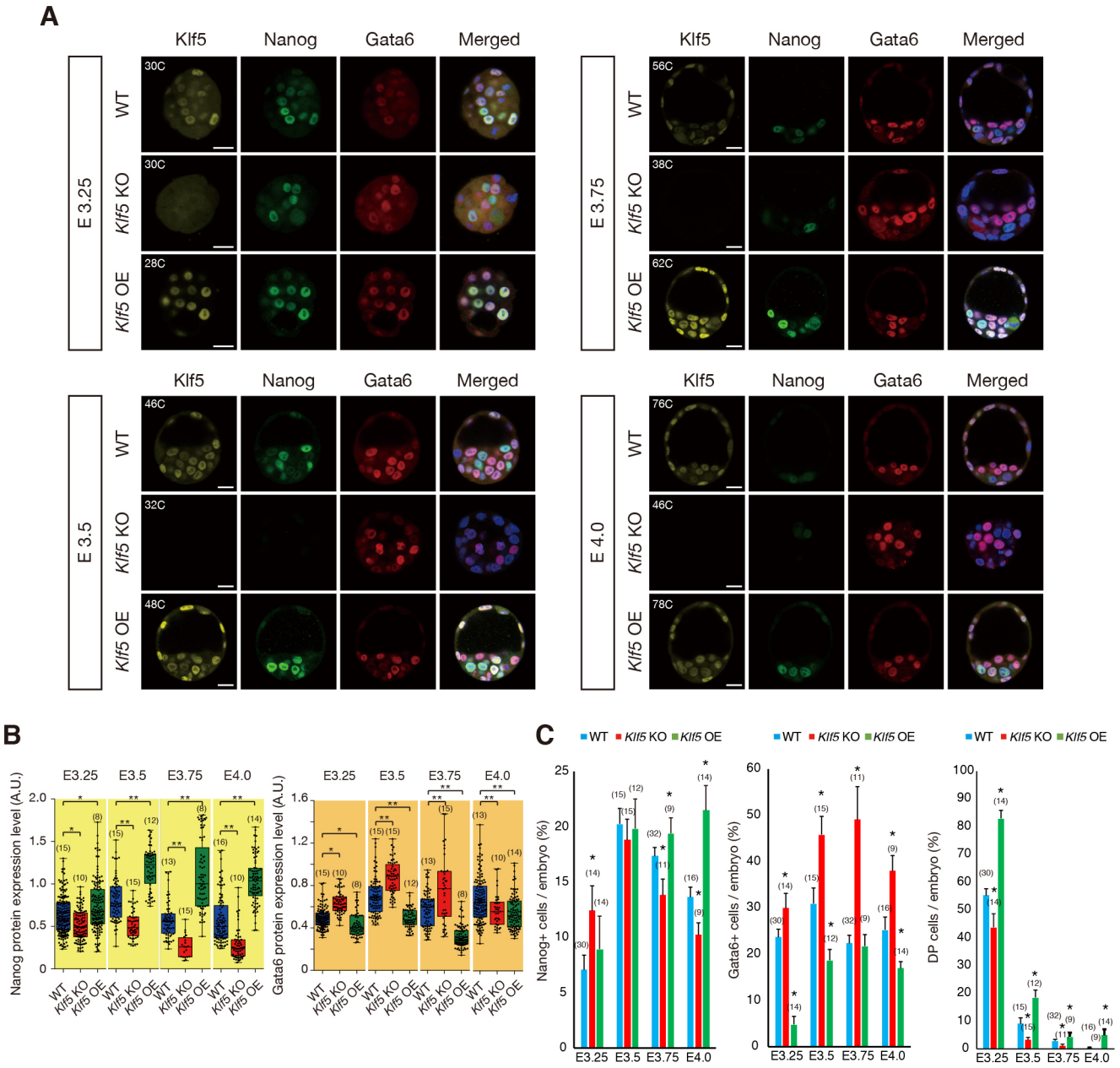

Fig. 1. Skewed EPI and PrE lineage specification in *Klf5* KO and OE blastocysts. (A) Expression levels of Nanog and Gata6 in WT, *Klf5* KO and *Klf5* OE mouse embryos from E3.25-4.0. Confocal microscopy transverse sections are shown. Note that Nanog expression was reduced in *Klf5* KO blastocysts at E3.25 and was dramatically reduced after E3.5. Gata6 expression was induced at E3.25-E4.0. C, cell number. Scale bars: 20 µm. (B) Tukey box plots of Nanog and Gata6 protein expression levels. Embryo numbers are shown in parentheses. A.U., arbitrary unit. The central mark is the median, the edges of the box are the 25th and 75th percentiles, and the whiskers extend to 1.5× the interquartile range. (C) Percentage of Nanog^{+} (Nanog^{+}/Gata6^{-}), Gata6^{+} (Nanog^{-}/Gata6^{+}) and DP cells per embryo. *P<0.01, **P<0.001, versus WT (Mann–Whitney U-test). Embryo numbers are shown in parentheses.

Klf5 KO embryos showed a cell proliferation defect (Fig. S1I) we categorised embryos by similar total cell numbers (<32 or 32-64) from various days of development and reached the same conclusion (Fig. S2B-D).

When we investigated Nanog and Gata6 expression in *Klf5* OE embryos at E3.25, *Klf5* OE blastocysts showed overall coexpression of Nanog and Gata6 (Fig. 1A). The numbers of DP cells per embryo at E3.5 to E4.0 were significantly increased in *Klf5* OE embryos (Fig. 1C, Fig. S2C,D). Whereas there were Gata6^{+} endoderm layers and Nanog^{+} EPI cells in WT blastocysts at E4.5, there were still significant numbers of DP cells centrally located towards presumably uncommitted cells in *Klf5* OE blastocysts at E4.5 (Fig. S2A,A′).

Accelerated PrE lineage specification in *Klf5* KO embryos

Specification of the PrE lineage involves Gata6, followed by sequential activation of Pdgfra, Sox17, Gata4 and Sox7 (Artus et al., 2010, 2011; Kang et al., 2013; Plusa et al., 2008). Sox17 is activated between the 32-cell and 64-cell stages (Artus et al., 2011; Morris et al., 2010; Niakan et al., 2010); Gata4 expression marks the onset of the mutual exclusion of Gata6 and Nanog and is activated at the 64-cell stage (Artus et al., 2011; Grabarek et al., 2012). Because we observed a reduction in the percentage of Nanog^{+} cells and an increase in Gata6^{+} cells in *Klf5* KO embryos at E3.75, we tested whether inner cells at E3.0 already exhibit signs of accelerated PrE lineage specification. Immunohistochemistry did not show any

Development (2017) 144, 3706-3718 doi:10.1242/dev.150755

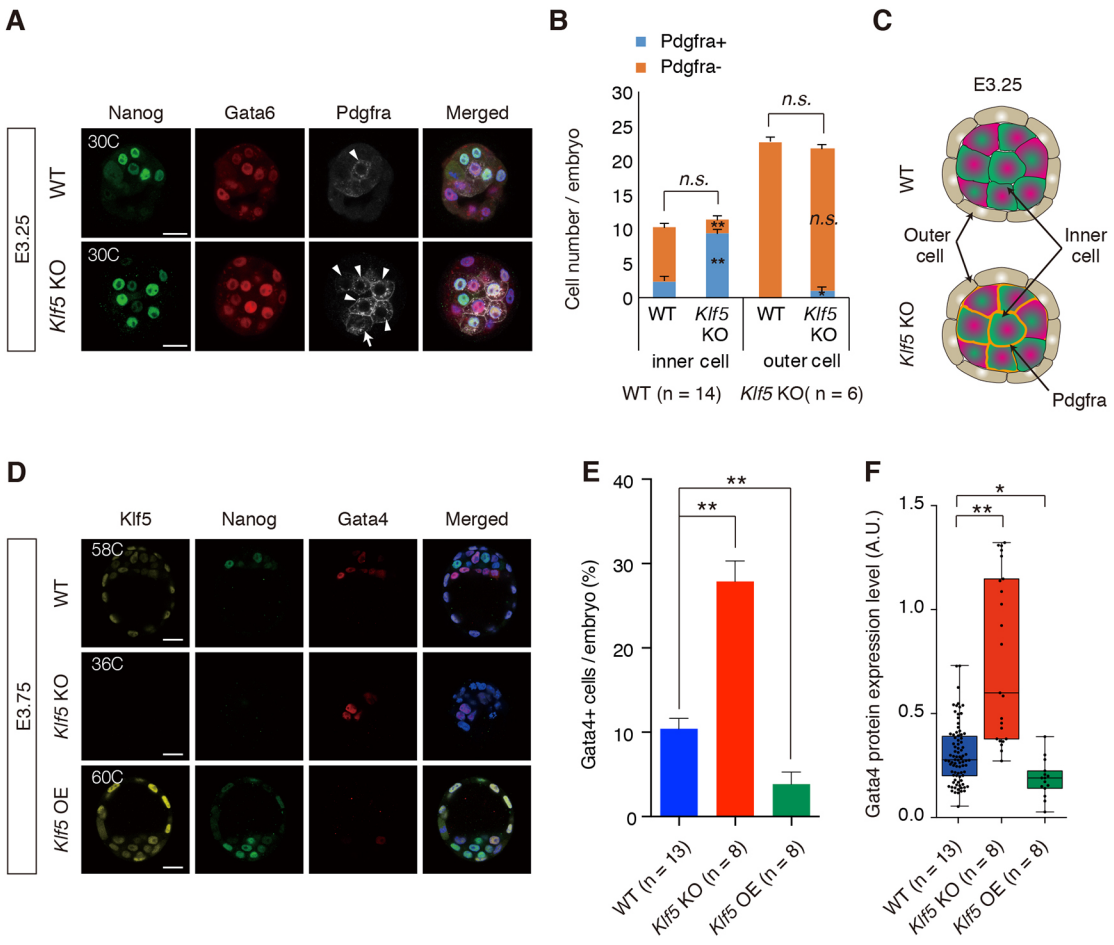

Fig. 2. Accelerated PrE lineage specification in *Klf5* KO embryos. (A) Upregulation of Pdgfra in the inner cells of *Klf5* KO embryos at E3.25. Note that the inner cells of the *Klf5* KO embryos were DP cells that strongly express Pdgfra. Arrowheads and arrow indicate inner cells and outer cells, respectively. Confocal microscopy transverse sections at E3.25 are shown. C, cell number. (B) Absolute number of Pdgfra$^+$ and Pdgfra$^-$ cells in inner or outer cells. (C) Illustration of WT and *Klf5* KO embryos at E3.25. More than 80% of inner cells in *Klf5* KO embryos strongly expressed Pdgfra (indicated by the orange outline of the cell membrane), but not in WT embryos, indicating accelerated PrE specification of the inner cells. (D) Expression of Nanog and Gata4 in WT and *Klf5* KO blastocysts from E3.75. Gata4 expression levels were dramatically upregulated in *Klf5* KO blastocysts. Confocal microscopy transverse sections are shown. (E) Percentage of Gata4$^+$ cells per embryo. (F) Tukey box plots of Gata4 protein expression levels. Embryo numbers are shown in parentheses. A.U., arbitrary unit. **P*<0.01, ***P*<0.001 (Fig. 2B: Fisher's exact test; Fig. 2E,F: Mann–Whitney *U*-test); n.s., not significant. Scale bars: 20 µm.

detectable Pdgfra or Sox17 protein expression in *Klf5* KO morulae at E3.0 (data not shown; Fig. S3A). However, at E3.25, immunohistochemistry showed strong Pdgfra expression in most of the inner cells of *Klf5* KO embryos but not WT embryos (Fig. 2A). Quantitation of Pdgfra$^+$ cells indicated that over 80% of the inner cells of *Klf5* KO embryos were Pdgfra$^+$, whereas fewer than 20% of the inner cells of WT embryos were Pdgfra$^+$ (Fig. 2B). It is of note that a small increase in Pdgfra$^+$ cells was observed in the outer cells of *Klf5* KO embryos (Fig. 2B). Taken together, the data revealed that the inner cells of *Klf5* KO embryos exhibit accelerated PrE lineage specification as early as E3.25 (Fig. 2C).

We also found an increase in the percentage of Sox17$^+$ cells in *Klf5* KO blastocysts at E3.5 (Fig. S3B-D), which was consistent with a previous report (Lin et al., 2010). Furthermore, we found an increase in the numbers of Gata4$^+$ cells in *Klf5* KO blastocysts at E3.75, which was in sharp contrast with the small number of cells found in *Klf5* OE embryos (Fig. 2D,E). Gata4 protein expression levels were increased in *Klf5* KO embryos and decreased in *Klf5* OE embryos (Fig. 2F). Collectively, these data indicated that *Klf5* KO embryos show an accelerated PrE lineage specification in the ICM.

During maturation of EPI cells at E4.25-4.5, it has been demonstrated that downregulation of Nanog expression is a hallmark of the naïve-to-primed transition of EPI cells (Kang et al., 2017; Saiz et al., 2016; Smith, 2017). Elevated Nanog expression in *Klf5* OE embryos from E3.25 to E4.25 suggests that these cells might remain in a naïve state and fail to differentiate into mature EPI cells. To examine the consequence of ubiquitous overexpression of *Klf5*, *Klf5* OE embryos at E5.5 (egg cylinder stage) were dissected and subjected to immunohistochemistry. In WT embryos, Klf5 protein was expressed in extra-embryonic ectoderm cells but not in EPI cells; however, *Klf5* OE embryos still expressed Klf5 protein in all cell lineages, including EPI cells (Fig. S4). Thus, the elevated Nanog expression caused by *Klf5* OE did not block differentiation into EPI cells. Yamanaka and colleagues indicated that even though *Fgf4* heterozygous embryos exhibit a reduction in the number of PrE cells, the embryos eventually develop normally (Krawchuk et al., 2013). Thus, although lower activity of the Fgf4-Fgfr-ERK pathway affects PrE maturation it is restored during development. We presume that the PrE maturation of *Klf5* OE embryos is restored, as seen in *Fgf4* heterozygous embryos. *Klf5* OE embryos developed normally until

Development (2017) 144, 3706-3718 doi:10.1242/dev.150755

E8.0 but then died at E11.5 for unknown reasons, while *Klf5* KO embryos showed reduced Cdx2 expression and failed to promote blastocoel expansion, indicating a defect in TE development. Taken together, these results indicated that loss or overexpression of *Klf5* results in skewed cell fate specification in the EPI/PrE lineages during preimplantation development.

Overactivation of the Fgf4-Fgfr-ERK pathway in *Klf5* KO embryos

To elucidate the molecular mechanism involved in the accelerated PrE lineage specification of *Klf5* KO embryos, microarray analyses were performed using amplified cDNAs from WT embryos and *Klf5* KO embryos at E3.0 (Fig. S5A), which at this stage showed no apparent defects and had normal expression levels of *Oct3/4*, *Nanog*, *Sox2* and *Cdx2* mRNAs (Fig. S5B). Bioinformatic analysis indicated that *Fgf4* expression was upregulated in *Klf5* KO embryos, whereas *Spry4*, a negative regulator of FGF-induced ERK activation, was downregulated (Fig. 3A). *Pdgfra* and *Sox17*, markers for the PrE lineage, were upregulated in *Klf5* KO embryos (Fig. 3A). In agreement with these observations, quantitative reverse-transcription PCR (RT-qPCR) analysis confirmed that *Fgf4*, *Pdgfra* and *Sox17* were significantly upregulated in *Klf5* KO embryos at E3.0 (Fig. 3B). Quantification of Sox17 immunostaining in *Klf5* KO embryos showed increased

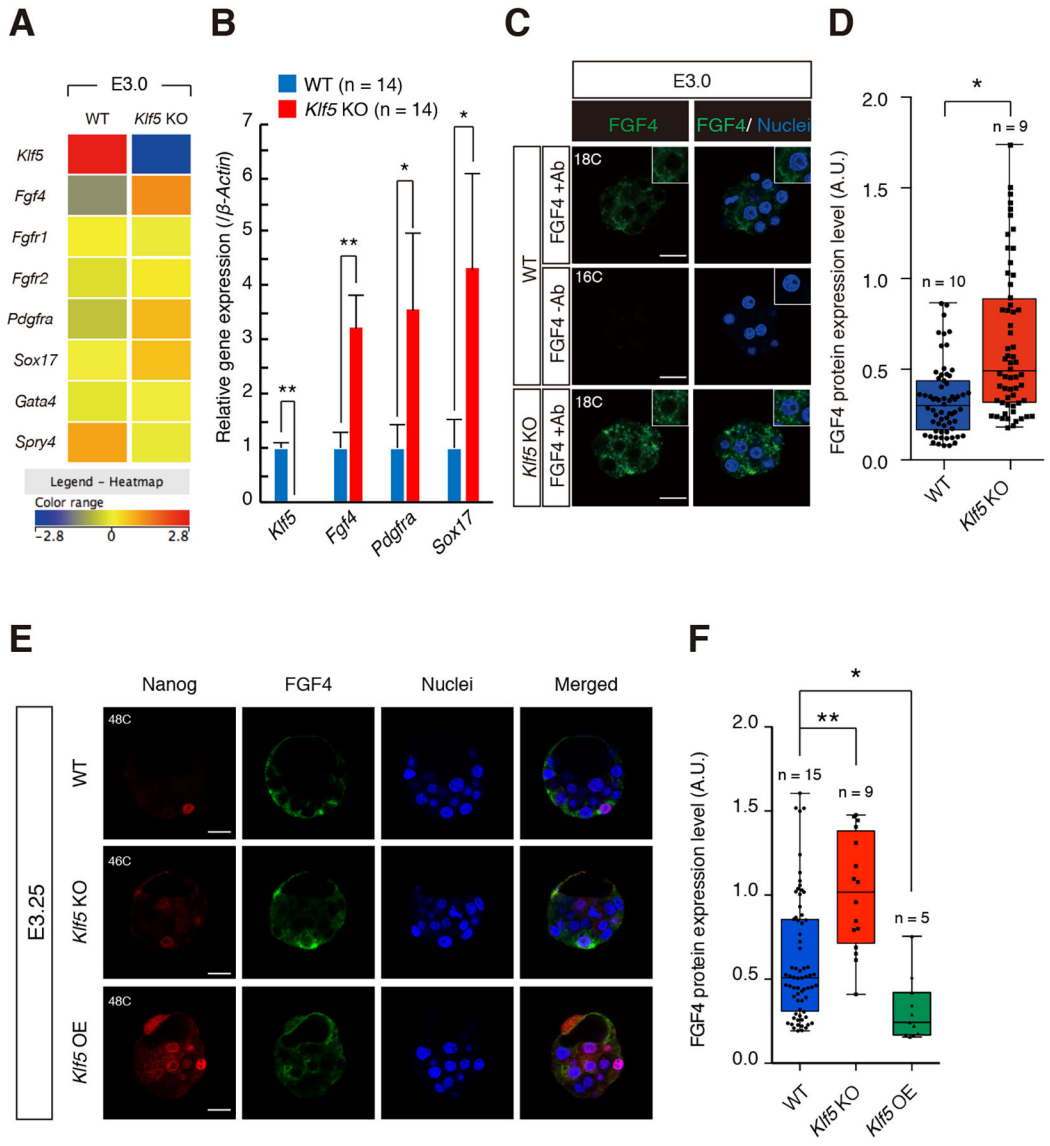

Fig. 3. *Klf5* is required for the repression of *Fgf4* expression in morulae at E3.0. (A) Heat map summarizing expression data for representative genes involved in Fgf4-ERK signalling and PrE specification. Colour intensity represents the mean-centered log2 expression; deeper red is associated with greater relative gene expression, and deeper blue is associated with decreased relative gene expression. (B) Average of relative gene expression in *Klf5* KO embryos compared with WT embryos at E3.0. β-actin was used for the normalisation of mRNA expression. **P*<0.05, ***P*<0.01 (Mann–Whitney *U*-test). (C) Increased expression levels of FGF4 protein in *Klf5* KO morulae at E3.0. Confocal transverse sections are shown. Insets are high-magnification images of FGF4$^+$ cells. Data are also shown for a negative control experiment on WT morulae without anti-FGF4 antibody (–Ab). C, cell number. (D) Tukey box plots showing FGF4 protein expression levels in FGF4$^+$ cells of WT and *Klf5* KO morulae at E3.0. **P*<0.01 (Mann–Whitney *U*-test). (E) FGF4 protein expression levels in FGF4$^+$ cells of WT, *Klf5* KO and *Klf5* OE blastocysts at E3.25. Confocal transverse sections are shown. (F) Tukey box plots showing FGF4 protein expression levels in FGF4$^+$ cells of WT, *Klf5* KO and *Klf5* OE embryos at E3.25. **P*<0.05, ***P*<0.01 (Mann–Whitney *U*-test). A.U., arbitrary unit. Scale bars: 20 µm.

Development (2017) 144, 3706-3718 doi:10.1242/dev.150755

numbers of Sox17$^+$ cells per embryo, as well as increased staining for Sox17 on a per-cell level at E3.5 (Fig. S3C,D). Therefore, the upregulation of PrE genes in the microarray analysis appears to reflect a combination of increased PrE cells per embryo and, in some cases such as *Sox17*, an increased level of PrE gene expression per cell.

To examine FGF4 protein expression in *Klf5* KO embryos, we validated an anti-FGF4 antibody by staining mouse *Fgf4* KO and WT ESCs and found that it could exclusively recognise endogenous FGF4 protein expressed in these cells (Fig. S5C). We further validated the anti-FGF4 antibody by staining the Nanog$^+$ EPI cells of WT blastocysts at E3.75 (Fig. S5D) and found that the staining pattern was consistent with a previous report by Frankenberg et al. (2011). Immunohistochemical analysis with this antibody confirmed that FGF4 was abundantly expressed in *Klf5* KO embryos at E3.0 and E3.25 (Fig. 3C-F). By contrast, FGF4 expression was significantly reduced in *Klf5* OE embryos at E3.25, indicating that Klf5 suppresses *Fgf4* (Fig. 3E,F). Since *Fgf4* encodes a secreted protein, it is difficult to identify *Fgf4*-expressing cells. To resolve this issue, we performed single-cell RT-qPCR analysis with amplified cDNA prepared from individual blastomeres of inner cells of WT, *Klf5* KO and *Klf5* OE embryos at E3.25 using the single-cell mRNA 3-prime end sequencing (SC3-seq) method (Nakamura et al., 2015) (Fig. 4A). There were two populations: *Fgf4*-high inner cells and *Fgf4*-low/negative inner cells. Given that *Pdgfra*, *Fgfr2* and *Sox17* are expressed in *Fgf4*-low/negative inner cells but not in *Fgf4*-high inner cells, these populations might represent PrE and EPI cells, respectively (Fig. 4A). There was no significant difference in the expression pattern of major lineage markers, such as *Nanog*, *Gata6*, *Oct3/4* and *Sox2*, between WT, *Klf5* KO and *Klf5* OE embryos (Fig. 4A). Importantly, the proportion of *Fgf4*-high inner cells to *Fgf4*-low/negative inner cells was significantly increased in *Klf5* KO embryos at E3.25 (Fig. 4B,C). Interestingly, *Fgf4* mRNA was significantly upregulated in *Fgf4*-high inner cells of *Klf5* KO embryos but downregulated in *Fgf4*-high inner cells of *Klf5* OE embryos, as compared with those of WT embryos (Fig. 4B,D). These results clearly demonstrated that *Klf5* suppresses *Fgf4* in *Fgf4*-high inner cells at E3.0-3.25.

To investigate whether *Klf5* directly regulates *Fgf4*, we surveyed the genomic binding sites of *Klf5* by examining public ChIP-seq data and found that three candidate regions in *Fgf4* loci were occupied by Klf5 in mouse ESCs (Fig. 4E). To verify this result, we established ESC lines that overexpressed epitope-tagged Klf5 and confirmed that the tagged protein binds to the three regions of *Fgf4* (Fig. 4F) and to the promoter and enhancer regions of *Nanog* (Jeon et al., 2016). These data suggest that Klf5 represses *Fgf4* through direct regulation. Although inner cells at E3.25 express *Fgfr2* homogeneously, *Fgf4* was observed to be expressed at two distinct levels, namely high and low, in populations of cells (Guo et al., 2010; Kurimoto et al., 2006; Ohnishi et al., 2014). However, the regulatory mechanism of *Fgf4* at early stages, such as in the morula, is unknown (Chazaud and Yamanaka, 2016). To the best of our knowledge, we are the first to identify *Klf5* as a crucial regulator of *Fgf4* at E3.0-3.25.

Of note, although *cis*-regulatory regions in the *Fgf4* promoter and enhancers are occupied by Klf5 (Fig. 4E,F), a lack of *Klf5* expression did not significantly alter *Fgf4* expression in mouse ESCs (Fig. S5E). This finding suggests a minor role for *Klf5* in the transcription of *Fgf4* in mouse ESCs, in contrast to its strongly suppressive role on *Fgf4* at E3.0 or E3.25. Previous work showed that Klf5 is a context-dependent transcription factor and, depending on the co-factor or nuclear environment, behaves as a transcriptional repressor or activator on the same set of genes (Oishi et al., 2008). Therefore, the different outcomes of *Fgf4* transcription promoted by the absence of *Klf5* might result in a different cell type, i.e. inner cells at E3.0-3.25 versus mouse ESCs (equivalent to EPI cells at E4.25) (Boroviak et al., 2014).

Fgfr or MEK inhibitors reverse the skewed lineage specification of *Klf5* KO blastocysts

Our data indicate that *Klf5* KO blastocysts show cell proliferation defects and accelerated PrE specification (Fig. S1I, Figs 1 and 2), yet it is not clear whether the overactivation of Fgf4-Fgfr-ERK signalling is responsible for the cell proliferation defects and accelerated PrE lineage specification in *Klf5* KO embryos. In fact, Lin et al. (2010) reported no difference in the phosphorylated ERK (pERK) signal between WT and *Klf5* KO blastocysts. However, it is of note that careful and extensive immunohistochemical analyses showed that a strong background signal hampers the detection of pERK in preimplantation embryos (Frankenberg et al., 2011), whereas pERK signals can be observed reproducibly in whole embryos after E5.5 (Corson et al., 2003).

To examine whether Fgf4-Fgfr-ERK signalling is responsible for the phenotype of *Klf5* KO blastocysts, we used chemical inhibitors to block the kinase activities of Fgfr1/2 (SU5402) and MEK (PD0325901) (Fig. 5A). Morulae at E2.75 were collected and cultured for 24 h in the presence or absence of these inhibitors, and we found that *Klf5* KO embryos treated with either SU5402 or PD0325901 showed marked phenotypic rescue in terms of a normal morphology with an expanded blastocoel, indistinguishable from WT blastocysts (Fig. 5B). The number of cells per embryo was also increased but still significantly different from that of WT embryos, suggesting that *Klf5* regulates cell proliferation in part through an Fgf4-Fgfr-ERK-independent mechanism (Fig. 5C). The number of TUNEL$^+$ cells was reduced dramatically in the inhibitor-treated *Klf5* KO embryos and was similar to that of WT embryos (Fig. 5C). Notably, inhibitors of the JNK and p38 MAPK (Mapk14) pathways did not significantly rescue the cell cycle defects of *Klf5* KO blastocysts (Fig. S6), indicating that JNK and p38 MAPK are not involved in this process.

We also attempted to test whether excess FGF4 activity is sufficient to cause defective cell proliferation in WT embryos and found that culturing in the presence of FGF4 slightly increased the number of TUNEL$^+$ cells but did not significantly change total cell number (Fig. 5D,E). When *Klf5* OE embryos were cultured in the presence of saturated levels of FGF4 (1 µg/ml) from E2.5 to E3.75 (Fig. S7A), this did not change total cell number (Fig. S7B-D); however, Gata6 protein expression was significantly upregulated in FGF4-stimulated *Klf5* OE embryos (Fig. S7E).

To investigate whether the precocious activation of Fgf4-Fgfr-ERK signalling was responsible for the altered lineage specification of *Klf5* KO blastocysts, WT and *Klf5* KO morulae at E2.5 were collected and cultured for 24 or 48 h in the presence or absence of PD0325901 and were then subjected to immunohistochemistry (Fig. 6A). *Klf5* KO blastocysts cultured *in vitro* for 24 h from E2.5 showed reduced Nanog and increased Gata6 expression levels, as did the *Klf5* KO blastocysts at E3.5 (Fig. 6B,C). MEK inhibitor treatment dramatically reversed the alterations in Nanog and Gata6 expression levels (Fig. 6B,C). When *Klf5* KO morulae were treated with PD0325901 from E2.5 for 24 h, most of the ICM cells were Nanog$^+$ EPI-biased cells (Fig. 6B,C). By contrast, when *Klf5* KO morulae were treated with vehicle alone for 24 h from E2.5, most of the ICM cells were Gata6$^+$ PrE cells. Importantly, the percentage of Nanog$^+$ cells among the ICM cells of *Klf5* KO blastocysts cultured

Development (2017) 144, 3706-3718 doi:10.1242/dev.150755

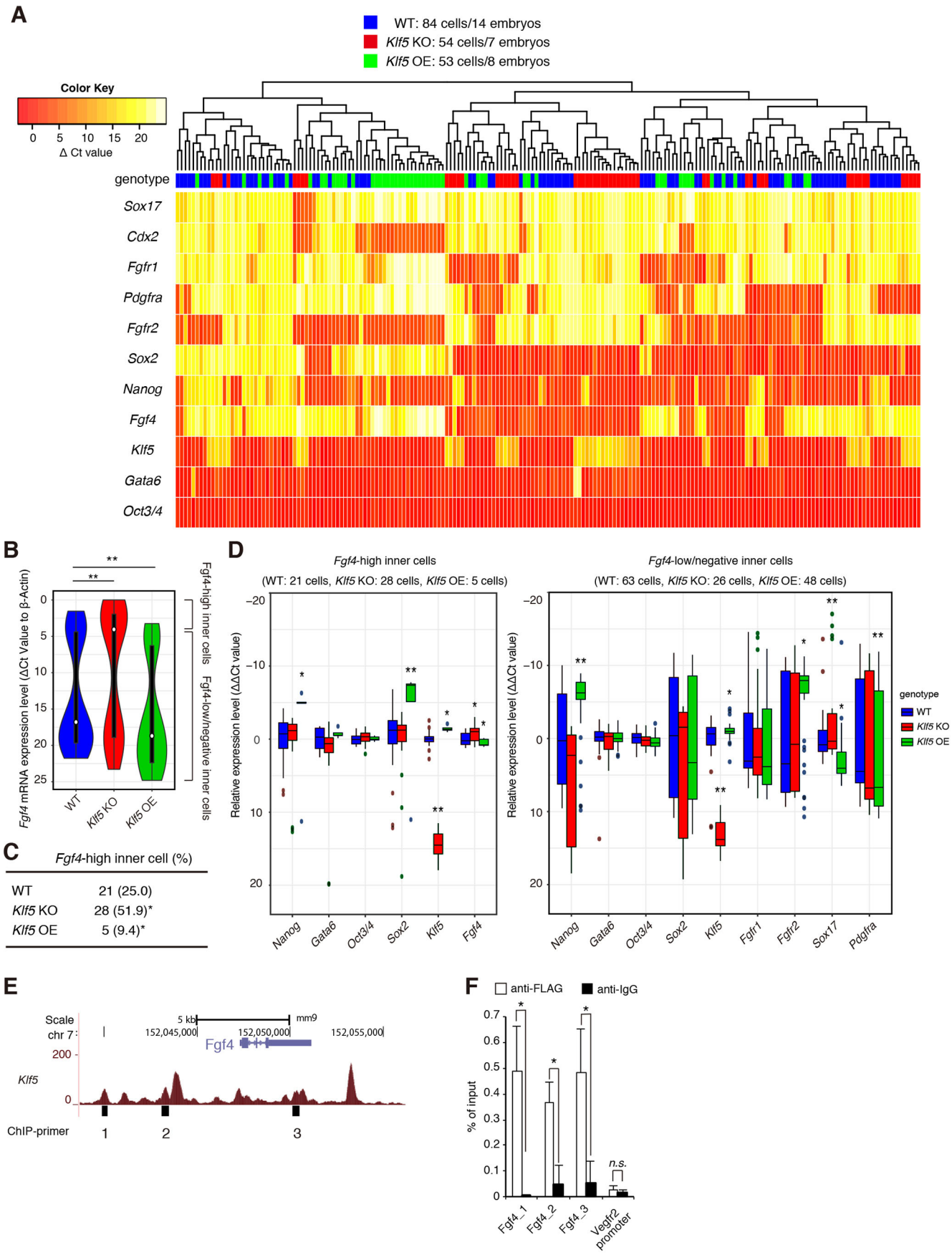

Fig. 4. See next page for legend.

Development (2017) 144, 3706-3718 doi:10.1242/dev.150755

Fig. 4. *Klf5* is required to suppress *Fgf4* in a subset of inner cells at E3.0-3.25. (A-C) Single-cell RT-qPCR analysis of inner cells from WT, *Klf5* KO and *Klf5* OE embryos at E3.25. cDNAs extracted from 84 cells from WT embryos (n=14), 54 cells from *Klf5* KO embryos (n=7) and 53 cells from *Klf5* OE embryos (n=8) were synthesised using the SC3-seq method. (A) The ΔCt values from the average Ct value of β-actin are shown as heat maps and are used for clustering. The genotype of each sample is shown above the heat map. (B) Violin plot of single-cell mRNA expression levels (ΔCt values from the average Ct value of β-actin) of *Fgf4* in WT, *Klf5* KO and *Klf5* OE inner cells at E3.25. Two cell populations can be distinguished by *Fgf4* expression level: *Fgf4*-high cells and *Fgf4*-low/negative cells, as determined by a ΔCt value of 4.3 that marks the 25th percentile expression levels in WT embryos. **P<0.001 (Mann–Whitney U-test). (C) Number of *Fgf4*-high cells among the inner cells of WT, *Klf5* KO and *Klf5* OE embryos at E3.25 from single-cell RT-qPCR as shown in A. *P<0.01, versus WT (Fisher's exact test). (D) ΔΔCt values normalised to the average WT ΔCt value of *Fgf4*-high and *Fgf4*-low/negative cells in WT, *Klf5* KO and *Klf5* OE embryos are shown as box plots. *Fgf4*-high cells were determined by a ΔCt value of 4.3 that marks the 25th percentile expression levels in WT embryos. Sample number is indicated above each boxplot. *P<0.01, **P<0.001 (Mann–Whitney U-test). (E) Binding peaks of Klf5 to *Fgf4* in mouse ESCs. Numbers below binding peaks indicate regions designated for ChIP primers used in F. (F) ChIP analysis of the binding of Klf5 to *Fgf4* in mouse ESCs. The promoter region of *Vegfr2*, which is not regulated by Klf5, was analysed as a negative control region. *P<0.01 (Student's t-test). n.s., not significant.

in the presence of PD0325901 was increased compared with WT, but was still less than that of PD0325901-treated WT embryos (Fig. 6C). When *Klf5* KO morulae were treated with PD0325901 from E2.5 for 48 h (corresponding to E4.5), all the cells in the ICM were Nanog$^+$ EPI cells (Fig. 6B′).

Because our previous results indicated that ESC lines could not be established from *Klf5* KO blastocysts and that *Klf5* was indispensable for ESC derivation from the ICM (Ema et al., 2008), we attempted to derive ESC lines from PD0325901-treated *Klf5* KO blastocysts. Sixty ESC lines were established and genotyped. Seven *Klf5* KO ESC lines were obtained (data not shown), demonstrating that treatment with this MEK inhibitor rescued the emergence of pluripotent EPI cells in *Klf5* KO blastocysts. By contrast, treatment with the MEK or Fgfr inhibitors did not affect the reduced expression of Cdx2 (Fig. S8). This suggested that the dysregulation of *Cdx2* in *Klf5* KO blastocysts was not caused by increased signalling through the Fgf4-Fgfr-ERK pathway but was nonetheless controlled by *Klf5*.

Taken together, our studies showed that the loss of *Klf5* results in the induction of *Fgf4* in morula at E3.0, followed by the rapid upregulation of Pdgfra in the inner cells at E3.25 and a decrease in Nanog$^+$ cells and DP cells at E3.5, which ultimately led to Gata6-expressing cells only. This skewed EPI/PrE phenotype with Gata6-only ICM cells was reversed by MEK inhibitors. However, overexpression of *Klf5* resulted in the reduction of *Fgf4* in blastocysts at E3.5 and an increase in Nanog$^+$ cells and DP cells at E3.5 or later, which ultimately led to the presence of DP 'uncommitted' cells by E4.0. Therefore, our model is that *Klf5* represses Fgf4-Fgfr-ERK signalling to suppress its precocious activation of the PrE specification programme, thus ensuring the emergence of Nanog$^+$ naïve pluripotent cells during development (Fig. 7).

DISCUSSION

Previous experiments showed that *Nanog* KO caused a severe reduction in *Fgf4* expression in blastocysts at E3.5, demonstrating that *Nanog* activates *Fgf4* expression in EPI precursor cells (Frankenberg et al., 2011; Messerschmidt and Kemler, 2010). Moreover, *Oct3/4* KO led to reduced *Fgf4* expression in blastocysts at E3.5 (Frum et al., 2013; Le Bin et al., 2014). Furthermore, mutant embryos lacking Sox2, which cooperates with Oct3/4 in the maintenance of ESC pluripotency, showed reduced *Fgf4* expression (Wicklow et al., 2014). Because Oct3/4-Sox2 complexes can directly induce *Fgf4* expression *in vitro* (Ambrosetti et al., 2000), there is an interplay between Nanog, Oct3/4 and Sox2 to regulate *Fgf4* for proper lineage segregation (Chazaud and Yamanaka, 2016). Thus, these studies showed that *Nanog* and *Oct3/4* activate *Fgf4* expression in EPI precursor cells at the E3.5 blastocyst stage; however, these studies did not address the regulatory mechanism of *Fgf4* at an earlier stage, such as the morula. The mechanism involved in the induction of *Fgf4* expression in a subset of inner cells at this stage is still unknown (Chazaud and Yamanaka, 2016). Our study demonstrated for the first time that *Klf5* is a crucial regulator for *Fgf4* in the morula at E3.0, before the blastocyst stage.

Bimodal *Fgf4* expression levels precede the exclusive production of Nanog and Gata6 (Guo et al., 2010; Ohnishi et al., 2014) and is the first sign of the segregation of the EPI and PrE lineages. However, what regulates *Fgf4* is unknown (Artus and Chazaud, 2014; Chazaud and Yamanaka, 2016). Yamanaka and colleagues clearly demonstrated that all ICM cells acquire a PrE fate when cultured in the presence of saturated levels of FGF4, and they proposed that the local concentration of FGF4 in the inner cells is important for the establishment of its salt-and-pepper distribution at the blastocyst stage (Yamanaka et al., 2010). At E3.0-3.25, DP inner cells exist as a common precursor pool and have the potential to commit to either fate asynchronously (Saiz et al., 2016). Activity of the Fgf4-Fgfr-ERK pathway regulates the balance of EPI and PrE differentiation from common precursors. We demonstrated that *Fgf4* expression is induced in a subset of *Fgf4*-high inner cells of *Klf5* KO embryos at E3.0-3.25. At that time, the number of DP cells was reduced in *Klf5* KO embryos. Furthermore, the skewed cell fate of *Klf5* KO embryos was markedly reversed by inhibitors of MEK and Fgfr. These results demonstrated that *Klf5* is involved in the segregation of the EPI and PrE lineages by suppressing precocious activation of the Fgf4-Fgfr-Fgfr-ERK pathway. Further examination of the mechanisms involved in the transcription of *Klf5* and the transcriptional activity of Klf5 protein could reveal how the bimodal expression of *Fgf4* is generated.

Given an elevation in Gata6 protein and *Sox17* mRNA expression in *Klf5* KO embryos at E3.0 or E3.25 (Fig. 1B, Fig. 3B, Fig. 4D), this might suggest a cell-autonomous role for Klf5 in the PrE lineage. However, the mRNA expression level of *Sox17* at E3.0 was much lower than that of other transcription factors such as Nanog, Sox2 and Gata6 (Sox17/Nanog ratio=5.6×10^{-6}, Sox17/Sox2=5.28×10^{-5}, Sox17/Gata6=0.00125), suggesting that *Sox17* mRNA expression is very low. Furthermore, we detected no Sox17 protein expression (Fig. S3A). This is consistent with previous reports that Sox17 is activated between the 32- and 64-cell stages in mouse embryos (Artus et al., 2011; Morris et al., 2010; Niakan et al., 2010). Thus, the elevation in *Sox17* mRNA expression in *Klf5* KO ICM is still too low to cause PrE differentiation. The Gata6 protein expression level also showed a slight increase (29%) at E3.25 (Fig. 1B), but the mRNA expression level of *Gata6* was not changed significantly between WT and *Klf5* KO embryos at E3.0 (Fig. S5B) and E3.25 (Fig. 4D), indicating that *Gata6* is not regulated by Klf5 at the transcriptional level at ∼E3.0-3.25. Taken together, these data suggest that Fgf4 regulates the induction of PrE differentiation, rather than there being a Sox17- or Gata6-mediated cell-autonomous mechanism.

Previous studies have demonstrated that Klf5 regulates lineage specification in TE and ICM (Ema et al., 2008; Lin et al., 2010).

Development (2017) 144, 3706-3718 doi:10.1242/dev.150755

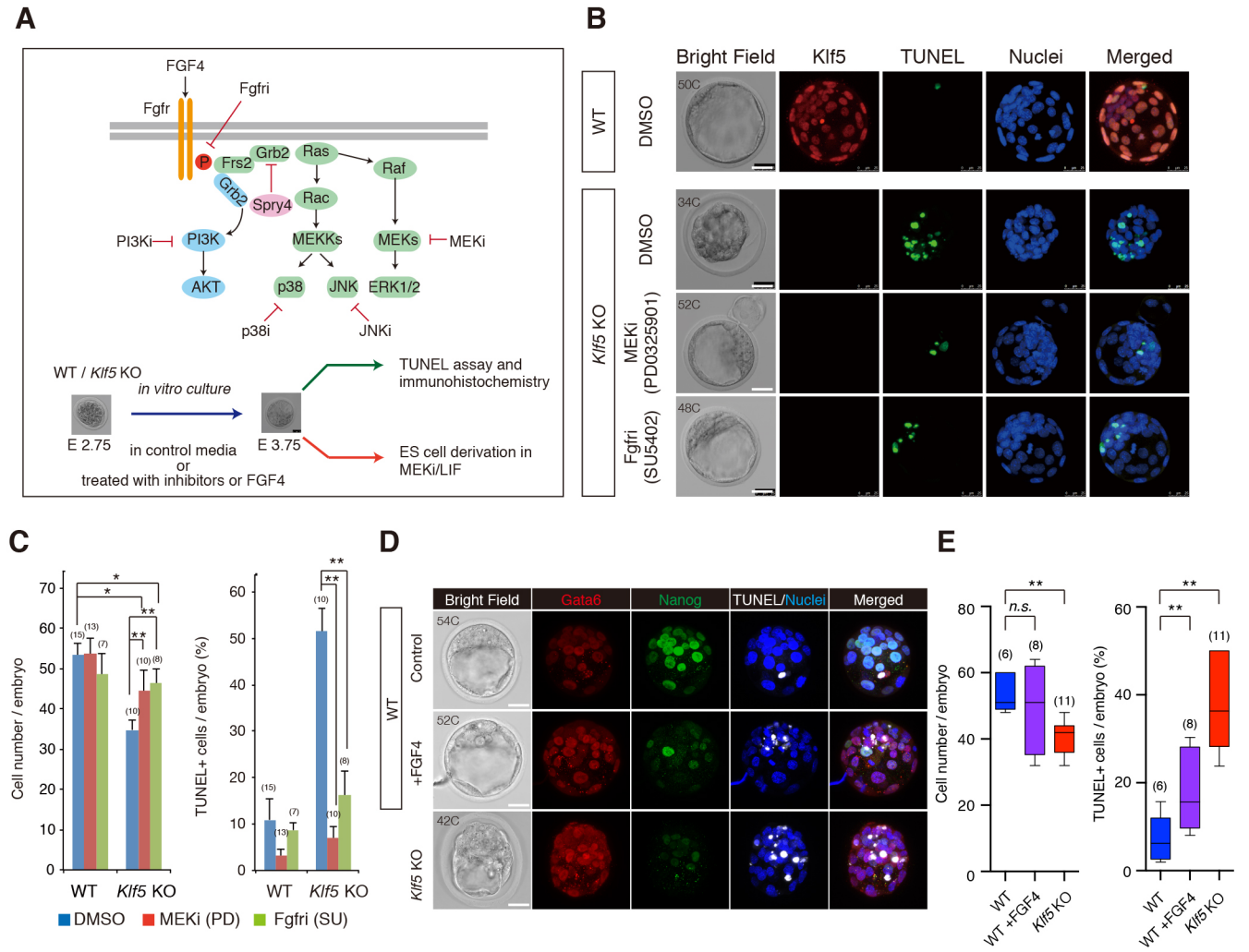

Fig. 5. Inhibition of Fgfr-ERK signalling rescues the cell cycle defects of *Klf5* KO blastocysts. (A) Experimental outline for assessing the role of the Fgf4-Fgfr-MAPK pathway in *Klf5* KO blastocysts. (B) Effects of inhibitors of MEK (MEKi) and Fgfr (Fgfri) in WT and *Klf5* KO blastocysts. Embryos at E2.75 were recovered and incubated in the presence or absence of MEKi (PD0325901, 1 µM) and Fgfri (SU5402, 2 µM) for 24 h, and then subjected to TUNEL assay and immunohistochemistry. *z*-projected confocal microscopy transverse sections are shown. C, cell number. Scale bars: 25 µm. (C) Number of cells (left) and percentages of TUNEL$^+$ (apoptotic) cells (right) per embryo. Embryo numbers are shown in parentheses. (D) Bright-field and fluorescent images of WT embryos cultured in the presence of FGF4 (1 µg/ml) from E2.75 to E3.75 and of *Klf5* KO embryos at E3.75. Maximum intensity projections of confocal microscopy images are shown. Scale bars: 20 µm. (E) WT embryos cultured in the presence of FGF4 showed a slight, but not significant, reduction in cell number (left) and increase in the percentage of TUNEL$^+$ cells (right). Embryo numbers are shown in parentheses. **P*<0.01, ***P*<0.001 (Mann–Whitney *U*-test).

While Klf5 directly regulates *Sox17* (Lin et al., 2010), it is still unclear how *Klf5* regulates the balance of EPI and PrE. Our results indicate that *Klf5* is required to suppress *Fgf4* in morula at E3.0, but it is not clear whether it continues to suppress *Fgf4* later in development because *Klf5* KO ESCs expressed normal levels of *Fgf4* (Fig. S5E). *Fgf4* and *Klf5* are expressed abundantly in such cells and are important for their differentiation and for self-renewal, respectively (Ema et al., 2008; Kunath et al., 2007). *Cis*-regulatory regions in the *Fgf4* promoter and enhancers are occupied by Klf5 in mouse ESCs (Fig. 4F). Nevertheless, the lack of *Klf5* expression did not significantly alter *Fgf4* expression (Fig. S5E). Therefore, we speculate that the transcriptional repression of *Fgf4* by *Klf5* occurs within a brief developmental window, such that the induction of *Fgf4* does not hamper the normal segregation of EPI and PrE lineages, and later *Klf5* expression does not repress *Fgf4* by the time the mature EPI cells arise. This is consistent with the observation that aggregation of *Klf5* KO ESCs with WT tetraploid embryos generates *Klf5* KO embryos that appear normal at E8.5, indicating that Klf5 is not required for normal development once the EPI is established (Ema et al., 2008).

Activation of the Fgf4-Fgfr-ERK pathway destabilises a naïve pluripotent state in mouse ESCs and promotes a primed state, whereas a reduction in ERK activity strongly promotes naïve pluripotency (Hamilton et al., 2013; Kunath et al., 2007; Ying et al., 2008). However, the precise molecular mechanisms of self-renewal promoted by ERK inhibition remain elusive. Although ERK inhibition contributes to self-renewal in part through the stabilisation of Klf2 and Klf4 proteins, which are subject to proteasome-dependent degradation of ERK-phosphorylated forms in mouse ESCs (Kim et al., 2012; Yeo et al., 2014), it is interesting to note that Klf5 modulates the level of pERK in mouse ESCs (T.A., unpublished observations). ERK inhibition also facilitates the emergence of naïve pluripotent cells in the blastocyst during murine development (Nichols et al., 2009). It remains unclear whether there is a specific physiological mechanism that mediates ERK inhibition to promote pluripotency *in vivo*, but Klf5 could be a key genetic

Development (2017) 144, 3706-3718 doi:10.1242/dev.150755

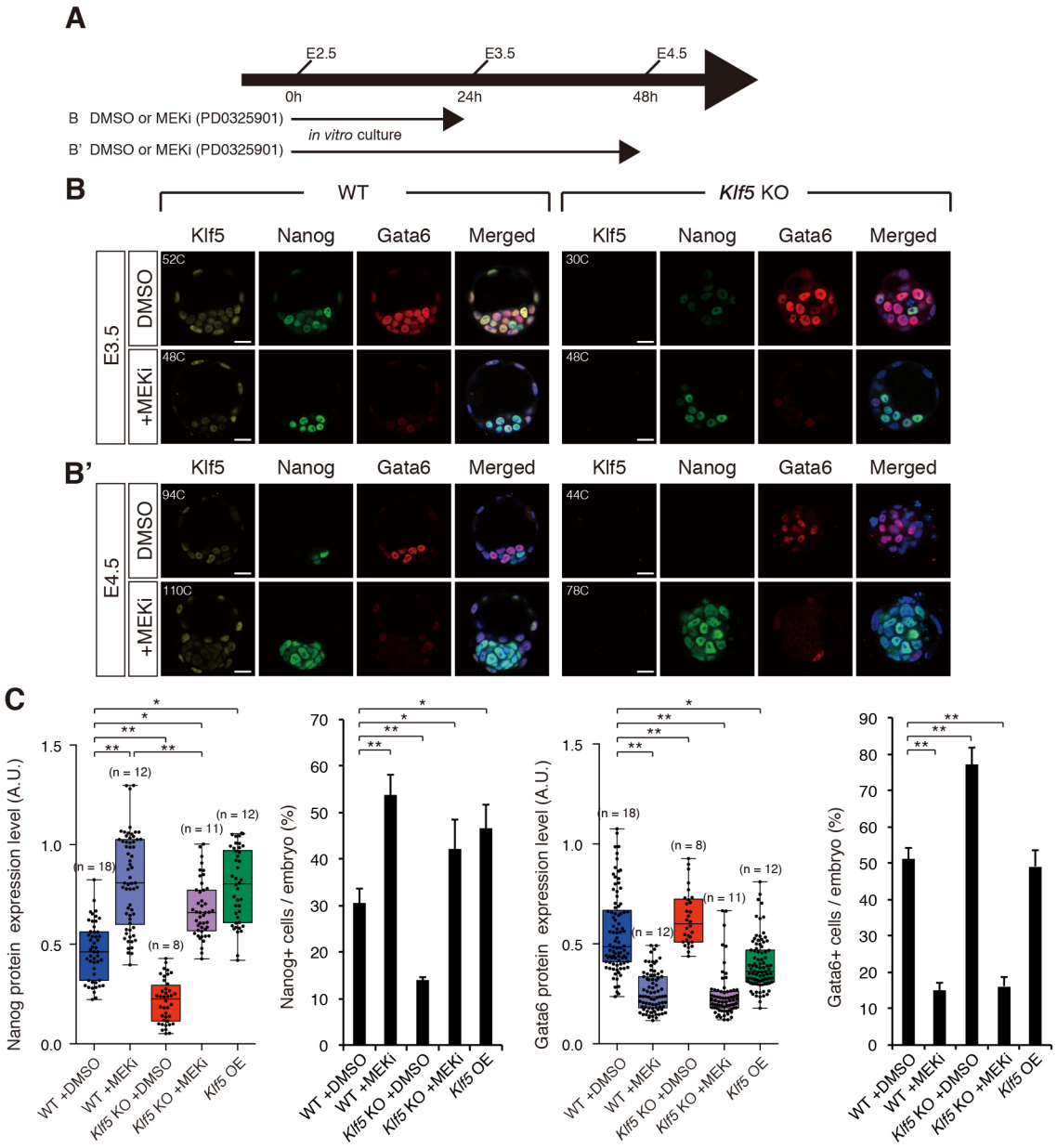

Fig. 6. Treatment with Fgfr or MEK inhibitors reverses the skewed lineage specification of *Klf5* KO blastocysts. (A) Experimental outline to assess the role of the Fgf4-Fgfr-ERK pathway in *Klf5* KO embryos. Embryos were collected from *Klf5* heterozygous intercrosses at E2.5 and cultured in the presence or absence of MEKi (PD0325901, 1 µM) for 24 h and 48 h. (B,B′) Effects of MEKi on skewed lineage specification of *Klf5* KO blastocysts at E3.5 (B) and E4.5 (B′). Confocal microscopy transverse sections are shown. C, cell number. Scale bars: 20 µm. (C) Tukey box plots of Nanog and Gata6 protein expression levels per embryo and the percentage of Nanog^{+} and Gata6^{+} cells per embryo. Embryo numbers are shown in parentheses. Mean and s.e.m. of three independent experiments. A.U., arbitrary unit. *P<0.01, **P<0.001 (Mann–Whitney U-test).

component in this regard. Further investigation of the functions of *Klf5* might allow us to understand how the symmetric expression of *Fgf4* and *Fgfr2* is altered during early development.

MATERIALS AND METHODS

Generation of *Klf5* KO and OE transgenic mice

Klf5$^{lacZ/lacZ}$ mice were generated as previously described (Ema et al., 2008). The *lacZ* cassette was inserted into the second exon of the *Klf5* gene. Conditional KO and OE alleles for *Klf5* were generated as described in the supplementary Materials and Methods. Primers used for the genotyping of the conditional KO and OE alleles for *Klf5* mice are described in Table S1. Mouse embryos were recovered at noon of the day on which the vaginal plug was discovered (considered E0.5).

Pluripotent stem cells

Mouse *Klf5*$^{+/+}$ (WT)::*Oct3/4-ireszeocinR* ESCs, *Klf5*$^{lacZ/lacZ}$ (KO)::*Oct3/4-ireszeocinR* ESCs and *Klf5*$^{+/+}$ (WT)::*Oct3/4-ireszeocinR*::Klf5 OE ESCs were generated as previously described (Ema et al., 2008) and were cultured in DMEM+15% Knockout Serum Replacement (KSR; Invitrogen). Details are provided in the supplementary Materials and Methods.

Manipulation of early embryos

Embryo manipulations were performed according to Nagy et al. (2003). For immunosurgery followed by ESC derivation, blastocysts were incubated with rabbit anti-mouse red blood cell antibody (Inter Cell Technologies, A3840; 1:8) for 10 min. After the blastocysts were briefly washed twice in M2, they were incubated with guinea pig serum (Calbiochem) for 15 min.

Development (2017) 144, 3706-3718 doi:10.1242/dev.150755

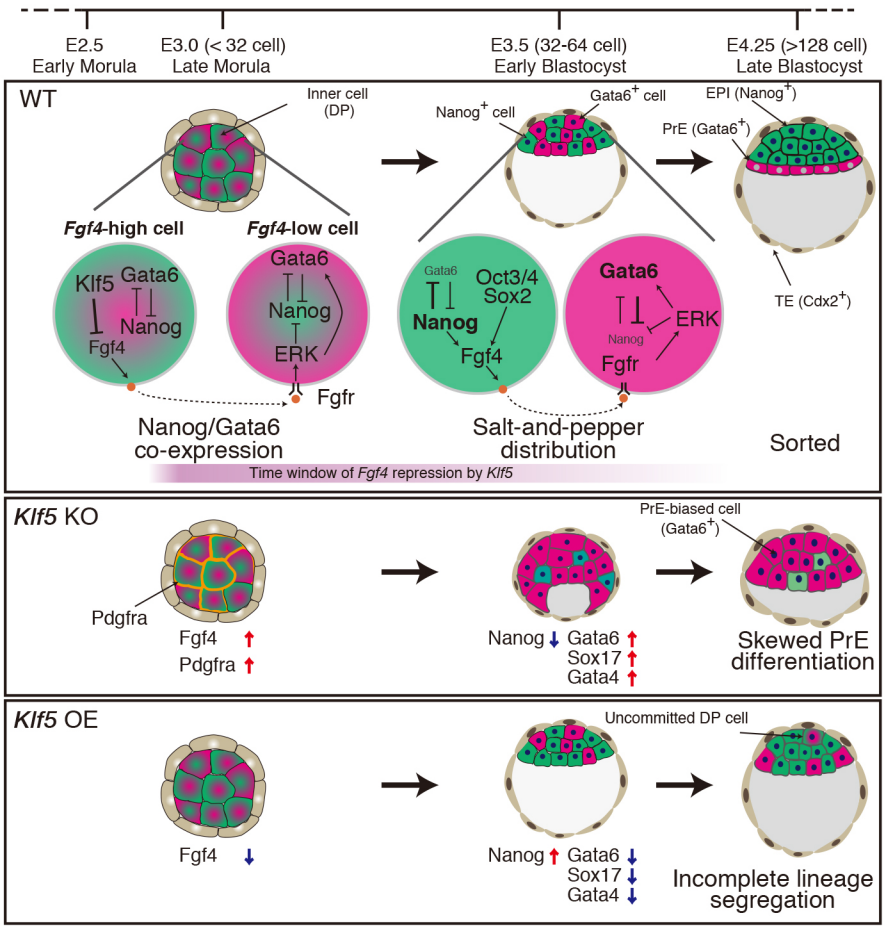

Fig. 7. Model for the role of *Klf5* in ICM lineage specification. At E3.0, the inner cells are DP precursors. At E3.5-3.75, the salt-and-pepper distribution of Nanog and Gata6 is evident, and cells are considered Nanog$^+$ EPI and Gata6$^+$ PrE lineage precursor cells. At E4.0-4.25, the lineages have been determined. Although Fgf4-ERK signalling is not involved in the initial coexpression of Nanog and Gata6, it regulates EPI/PrE specification by inhibiting Nanog and maintaining Gata6 expression. In the *Klf5* KO embryos, *Fgf4* is overexpressed because of derepression in the absence of *Klf5*, leading to PrE lineage specification. Gata4, a late marker for PrE lineage specification, is seen from the 64-cell stage in *Klf5* KO embryos but only in a few *Klf5* OE embryos, indicating accelerated differentiation into the PrE lineage. At E3.5, *Fgf4* is activated in EPI precursor cells in a Nanog- and Oct3/4-dependent manner [according to Frankenberg et al. (2011); Frum et al. (2013); Le Bin et al. (2014); Messerschmidt and Kemler (2010)]. Klf5 represses precocious *Fgf4* transcription to suppress the Fgf4-Fgfr-ERK pathway, thereby ensuring Nanog$^+$ pluripotent EPI development.

After removal of the zona pellucidae with acidic Tyrode's solution (Sigma-Aldrich), the cells were cultured in ESC medium for 2 weeks on a gelatine-coated dish. For *in vitro* culture of early mouse embryos, embryos at the 2-cell stage or later were incubated in KSOM (Millipore) in the presence or absence of PD0325901 (1 µM; Wako), SU5402 (2 µM; Wako), CHIR99021 (Chiron; 3 µM; Wako), JNK inhibitor II (5 µM; Calbiochem), SB203508 (10 µM; Calbiochem) or LY924002 (10 µM; Calbiochem). To activate the Fgf4-Fgfr-ERK pathway, recombinant human FGF4 (R&D Systems) was added at a saturated concentration (1 µg/ml) prepared in KSOM. 1 µg/ml heparin (Sigma) was added together with FGF4 or control. BrdU was added (10 µM; BD Pharmigen) for 2 h, and BrdU Flow Kits (BD Pharmingen) were used for detection.

Immunohistochemistry

Embryos were fixed in 4% paraformaldehyde (PFA) in PBS for 15 min, permeabilised in 0.5% Triton X-100 for 15 min and incubated in blocking reagent (PBS, 10% donkey serum, 0.1% BSA, 0.01% Tween 20) for 1 h. Embryos were incubated at 4°C overnight with primary antibodies prepared in blocking reagent. After the embryos were washed with PBS+0.5% Triton X-100, they were incubated with secondary antibodies in the blocking reagent for 3 h at 4°C. Nuclei were stained with Hoechst 33342 (10 µg/ml; Molecular Probes). Antibodies used for the immunohistochemistry are described in Table S2. Immunohistochemistry with anti-FGF4 antibody was performed as described in the supplementary Materials and Methods.

Confocal microscopy analysis and image data acquisition

Embryos were mounted in drops of 30% glycerol on glass-bottom dishes. Confocal images were acquired using a Leica TCS SP5 or SP8 camera. Fluorescence was excited with a 405 nm UV laser for Hoechst 33342, a 638 nm laser for Cy5 or Alexa Fluor 633, a 552 nm laser for Cy3, and a 488 nm laser for Alexa Fluor 488. Images were acquired using an HC PL APO CS2 40×/1.30 oil-immersion objective lens (Leica), with optical sections of 2-2.5 µm. A hybrid detector system (Leica) was used for the acquisition of raw images, which were processed using Leica software or Photoshop CS6 (Adobe). Cell nuclei were counted manually using ImageJ image analysis software (National Institutes of Health). Protein expression levels were analysed as described (Dietrich and Hiiragi, 2007; Kang et al., 2013). Briefly, mean fluorescence intensities inside regions of interest (for example, nuclei) were measured, and subtracted from background signals, which were defined as the average of the mean fluorescence intensities of randomly chosen cytoplasmic signals, and were then normalised against the mean fluorescence intensity in the Hoechst channel using ImageJ (Dietrich and Hiiragi, 2007). We defined a cell as positive if it showed a higher fluorescence signal than the background. To quantify Nanog and Gata6 protein expression levels, we measured Nanog expression in both Nanog$^+$/Gata6$^-$ and Nanog$^+$/Gata6$^+$ (DP) cells, and Gata6 expression in both Gata6$^+$/Nanog$^-$ and DP cells.

For the quantification of FGF4 expression in preimplantation embryos, background signals were subtracted from mean fluorescence intensities inside regions of interest in the cytoplasm of FGF4$^+$ cells. Background signals were defined as the average of the mean fluorescence intensities of randomly chosen cytoplasmic regions in without-antibody negative controls. FGF4 expression values were then normalised against the mean fluorescence intensity in the Hoechst channel using ImageJ. Individual cells were distinguished using intercellular gaps seen in differential interference contrast (DIC) images from the same focal plane as the corresponding confocal microscopy image.

TUNEL assay

Apoptotic cells were identified using the DeadEnd Fluorometric TUNEL System (Promega). For counting TUNEL$^+$ cells, individual cells were identified using the intercellular gaps seen in DIC images merged with images of nuclear staining and TUNEL staining. Fragmented or pyknotic nuclei bounded by the same intercellular gap were counted as one cell.

Development (2017) 144, 3706-3718 doi:10.1242/dev.150755

Chromatin immunoprecipitation (ChIP) assays

ChIP assays were performed as previously described (Ito et al., 2013). Cells were fixed with 1% formaldehyde and sonicated. The samples were incubated with normal mouse IgG and anti-FLAG-M2 antibody. For details, see the supplementary Materials and Methods. Primers used for ChIP-qPCR are listed in Table S3.

ChIP-sequencing (ChIP-seq) data analysis

To locate *Fgf4* loci occupied by Klf5 in mouse ESCs, ChIP-seq data of Aksoy et al. (2014) were analysed as described in the supplementary Materials and Methods.

Microarray analysis

cDNAs were synthesised from individual WT and *Klf5* KO embryos at E3.0 as previously described (Kurimoto et al., 2007; Nakamura et al., 2015). The cDNAs were amplified further in a linear fashion and labelled with a Cy3- or Cy5-conjugated nucleotide. Hybridisation procedures were performed by TaKaRa Bio. Raw data were analysed using GeneSpring software version 13.0 (Agilent Technologies). The raw probe intensities were background subtracted. Signal values were set to threshold level 10 and log2 transformed. Normalization was performed using a 75th percentile shift algorithm. Further normalization using baseline to median of all samples algorithm was performed. Transcripts were filtered with 2-fold expression change compared with the median intensity in all samples.

Isolation of single cells for cDNA amplification

Outer cells of E3.25 embryos were removed by immunosurgery. Inner cells were incubated in a 1:1 mixture of Accutase (Nakalai Tesque) and 0.25% trypsin-EDTA (Invitrogen) for ∼5 min at 37°C and then dissociated into single cells by pipetting. cDNAs were synthesised from the isolated single cell using the single-cell mRNA 3-prime sequencing (SC3-seq) method as previously described (Nakamura et al., 2015).

RT-qPCR analysis

First-strand cDNA was synthesised from total RNA using the QuantiTect Reverse Transcription Kit (Qiagen). Real-time PCR was performed with SYBR Premix Ex Taq II (TaKaRa) and analysed on a Thermal Cycler Dice Real-Time System (TP850; TaKaRa). The amount of target RNA was estimated using an appropriate standard curve and divided by the estimated amount of β-actin for normalisation. Primers used for RT-qPCR are listed in Table S3.

Statistical analysis

Statistical analyses were performed using the nonparametric Mann–Whitney *U*-test or Student's *t*-test. Data are expressed as the mean and s.e. Differences were considered significant at $P<0.05$. Statistical analyses were performed using Prism6 (GraphPad) for the nonparametric Mann–Whitney *U*-test and Excel (Microsoft) for Student's *t*-test. Single-cell qPCR data analysis was performed using R software with gplots (ver. 3.0.1) and ggplot2 (ver. 2.2.1) and Excel (Microsoft).

Acknowledgements

We thank Drs Hitoshi Niwa, Yojiro Yamanaka and Tomoyuki Tsukiyama for helpful discussions and reagents. M.E. thanks Dr Vincent Kelly for critical reading of the manuscript.

Competing interests

The authors declare no competing or financial interests.

Author contributions

Conceptualization: M.E., T.A.; Methodology: T.A., T.W., K.M., H.J., J.Y., I.M., R.N., T.K., T.N., K.K., M.S., S.T.; Software: T.W., M.M., T.N., K.K., M.S.; Validation: T.A.; Formal analysis: T.A.; Investigation: T.A., T.W., K.M., H.J., A.K.; Resources: I.M., R.N., T.K., S.T.; Data curation: T.A., T.K.; Writing - original draft: M.E., T.A.; Writing - review & editing: M.E., T.A., T.K.; Supervision: M.E.; Funding acquisition: M.E.

Funding

This work was supported in part by a grant from PRESTO, Japan Science and Technology Agency (JST) (to M.E.). This work was also supported by a Grant-in-Aid for Japan Society for the Promotion of Science (JSPS) Fellows (20057002 to T.A. and T.W.).

Data availability

Microarray data have been deposited at Gene Expression Omnibus under accession number GSE65020.

Supplementary information

Supplementary information available online at
http://dev.biologists.org/lookup/doi/10.1242/dev.150755.supplemental

References

Aksoy, I., Giudice, V., Delahaye, E., Wianny, F., Aubry, M., Mure, M., Chen, J., Jauch, R., Bogu, G. K., Nolden, T. et al. (2014). Klf4 and Klf5 differentially inhibit mesoderm and endoderm differentiation in embryonic stem cells. *Nat. Commun.* **5**, 3719.

Ambrosetti, D.-C., Schöler, H. R., Dailey, L. and Basilico, C. (2000). Modulation of the activity of multiple transcriptional activation domains by the DNA binding domains mediates the synergistic action of Sox2 and Oct-3 on the fibroblast growth factor-4 enhancer. *J. Biol. Chem.* **275**, 23387-23397.

Artus, J. and Chazaud, C. (2014). A close look at the mammalian blastocyst: epiblast and primitive endoderm formation. *Cell. Mol. Life Sci.* **71**, 3327-3338.

Artus, J., Panthier, J.-J. and Hadjantonakis, A.-K. (2010). A role for PDGF signaling in expansion of the extra-embryonic endoderm lineage of the mouse blastocyst. *Development* **137**, 3361-3372.

Artus, J., Piliszek, A. and Hadjantonakis, A.-K. (2011). The primitive endoderm lineage of the mouse blastocyst: sequential transcription factor activation and regulation of differentiation by Sox17. *Dev. Biol.* **350**, 393-404.

Bedzhov, I. and Zernicka-Goetz, M. (2015). Cell death and morphogenesis during early mouse development: are they interconnected? *BioEssays* **37**, 372-378.

Bessonnard, S., De Mot, L., Gonze, D., Barriol, M., Dennis, C., Goldbeter, A., Dupont, G. and Chazaud, C. (2014). Gata6, Nanog and Erk signaling control cell fate in the inner cell mass through a tristable regulatory network. *Development* **141**, 3637-3648.

Boroviak, T., Loos, R., Bertone, P., Smith, A. and Nichols, J. (2014). The ability of inner-cell-mass cells to self-renew as embryonic stem cells is acquired following epiblast specification. *Nat. Cell Biol.* **16**, 516-528.

Chan, Y.-S., Göke, J., Ng, J.-H., Lu, X., Gonzales, K. A. U., Tan, C.-P., Tng, W.-Q., Hong, Z.-Z., Lim, Y.-S. and Ng, H.-H. (2013). Induction of a human pluripotent state with distinct regulatory circuitry that resembles preimplantation epiblast. *Cell Stem Cell* **13**, 663-675.

Chazaud, C. and Yamanaka, Y. (2016). Lineage specification in the mouse preimplantation embryo. *Development* **143**, 1063-1074.

Chazaud, C., Yamanaka, Y., Pawson, T. and Rossant, J. (2006). Early lineage segregation between epiblast and primitive endoderm in mouse blastocysts through the Grb2-MAPK pathway. *Dev. Cell* **10**, 615-624.

Corson, L. B., Yamanaka, Y., Lai, K.-M. V. and Rossant, J. (2003). Spatial and temporal patterns of ERK signaling during mouse embryogenesis. *Development* **130**, 4527-4537.

Dietrich, J.-E. and Hiiragi, T. (2007). Stochastic patterning in the mouse pre-implantation embryo. *Development* **134**, 4219-4231.

Ema, M., Mori, D., Niwa, H., Hasegawa, Y., Yamanaka, Y., Hitoshi, S., Mimura, J., Kawabe, Y., Hosoya, T., Morita, M. et al. (2008). Krüppel-like factor 5 is essential for blastocyst development and the normal self-renewal of mouse ESCs. *Cell Stem Cell* **3**, 555-567.

Frankenberg, S., Gerbe, F., Bessonnard, S., Belville, C., Pouchin, P., Bardot, O. and Chazaud, C. (2011). Primitive endoderm differentiates via a three-step mechanism involving Nanog and RTK signaling. *Dev. Cell* **21**, 1005-1013.

Frum, T., Halbisen, M. A., Wang, C., Amiri, H., Robson, P. and Ralston, A. (2013). Oct4 cell-autonomously promotes primitive endoderm development in the mouse blastocyst. *Dev. Cell* **25**, 610-622.

Grabarek, J. B., Zyzyńska, K., Saiz, N., Piliszek, A., Frankenberg, S., Nichols, J., Hadjantonakis, A.-K. and Plusa, B. (2012). Differential plasticity of epiblast and primitive endoderm precursors within the ICM of the early mouse embryo. *Development* **139**, 129-139.

Guo, G., Huss, M., Tong, G. Q., Wang, C., Li Sun, L., Clarke, N. D. and Robson, P. (2010). Resolution of cell fate decisions revealed by single-cell gene expression analysis from zygote to blastocyst. *Dev. Cell* **18**, 675-685.

Hamilton, W. B., Kaji, K. and Kunath, T. (2013). ERK2 suppresses self-renewal capacity of embryonic stem cells, but is not required for multi-lineage commitment. *PLoS ONE* **8**, e60907.

Hermitte, S. and Chazaud, C. (2014). Primitive endoderm differentiation: from specification to epithelium formation. *Philos. Trans. R. Soc. Lond. B Biol. Sci.* **369**, pii: 20130537.

Ito, I., Waku, T., Aoki, M., Abe, R., Nagai, Y., Watanabe, T., Nakajima, Y., Ohkido, I., Yokoyama, K., Miyachi, H. et al. (2013). A nonclassical vitamin D receptor pathway suppresses renal fibrosis. *J. Clin. Invest.* **123**, 4579-4594.

Jeon, H., Waku, T., Azami, T., Khoa, L. T. P., Yanagisawa, J., Takahashi, S. and Ema, M. (2016). Comprehensive identification of Krüppel-like factor family members contributing to the self-renewal of mouse embryonic stem cells and cellular reprogramming. *PLoS ONE* **11**, e0150715.

Jiang, J., Chan, Y.-S., Loh, Y.-H., Cai, J., Tong, G.-Q., Lim, C.-A., Robson, P., Zhong, S. and Ng, H.-H. (2008). A core Klf circuitry regulates self-renewal of embryonic stem cells. *Nat. Cell Biol.* **10**, 353-360.

Kang, M., Piliszek, A., Artus, J. and Hadjantonakis, A.-K. (2013). FGF4 is required for lineage restriction and salt-and-pepper distribution of primitive endoderm factors but not their initial expression in the mouse. *Development* **140**, 267-279.

Kang, M., Garg, V. and Hadjantonakis, A.-K. (2017). Lineage establishment and progression within the inner cell mass of the mouse blastocyst requires FGFR1 and FGFR2. *Dev. Cell* **41**, 496-510.e5.

Kim, M. O., Kim, S.-H., Cho, Y.-Y., Nadas, J., Jeong, C.-H., Yao, K., Kim, D. J., Yu, D.-H., Keum, Y.-S., Lee, K.-Y. et al. (2012). ERK1 and ERK2 regulate embryonic stem cell self-renewal through phosphorylation of Klf4. *Nat. Struct. Mol. Biol.* **19**, 283-290.

Krawchuk, D., Honma-Yamanaka, N., Anani, S. and Yamanaka, Y. (2013). FGF4 is a limiting factor controlling the proportions of primitive endoderm and epiblast in the ICM of the mouse blastocyst. *Dev. Biol.* **384**, 65-71.

Kunath, T., Saba-El-Leil, M. K., Almousailleakh, M., Wray, J., Meloche, S. and Smith, A. (2007). FGF stimulation of the Erk1/2 signalling cascade triggers transition of pluripotent embryonic stem cells from self-renewal to lineage commitment. *Development* **134**, 2895-2902.

Kurimoto, K., Yabuta, Y., Ohinata, Y., Ono, Y., Uno, K. D., Yamada, R. G., Ueda, H. R. and Saitou, M. (2006). An improved single-cell cDNA amplification method for efficient high-density oligonucleotide microarray analysis. *Nucleic Acids Res.* **34**, e42.

Kurimoto, K., Yabuta, Y., Ohinata, Y. and Saitou, M. (2007). Global single-cell cDNA amplification to provide a template for representative high-density oligonucleotide microarray analysis. *Nat. Protoc.* **2**, 739-752.

Le Bin, G. C., Muñoz-Descalzo, S., Kurowski, A., Leitch, H., Lou, X., Mansfield, W., Etienne-Dumeau, C., Grabole, N., Mulas, C., Niwa, H. et al. (2014). Oct4 is required for lineage priming in the developing inner cell mass of the mouse blastocyst. *Development* **141**, 1001-1010.

Lin, S.-C. J., Wani, M. A., Whitsett, J. A. and Wells, J. M. (2010). Klf5 regulates lineage formation in the pre-implantation mouse embryo. *Development* **137**, 3953-3963.

Messerschmidt, D. M. and Kemler, R. (2010). Nanog is required for primitive endoderm formation through a non-cell autonomous mechanism. *Dev. Biol.* **344**, 129-137.

Morris, S. A., Teo, R. T. Y., Li, H., Robson, P., Glover, D. M. and Zernicka-Goetz, M. (2010). Origin and formation of the first two distinct cell types of the inner cell mass in the mouse embryo. *Proc. Natl. Acad. Sci. USA* **107**, 6364-6369.

Nagy, A., Gertsenstein, M., Vintersten, K. and Behringer, R. (2003). *Manipulating the Mouse Embryo*. Cold Spring Harbor, NY: Cold Spring Harbor Laboratory Press.

Nakamura, T., Yabuta, Y., Okamoto, I., Aramaki, S., Yokobayashi, S., Kurimoto, K., Sekiguchi, K., Nakagawa, M., Yamamoto, T. and Saitou, M. (2015). SC3-seq: a method for highly parallel and quantitative measurement of single-cell gene expression. *Nucleic Acids Res.* **43**, e60.

Niakan, K. K., Ji, H., Maehr, R., Vokes, S. A., Rodolfa, K. T., Sherwood, R. I., Yamaki, M., Dimos, J. T., Chen, A. E., Melton, D. A. et al. (2010). Sox17 promotes differentiation in mouse embryonic stem cells by directly regulating extraembryonic gene expression and indirectly antagonizing self-renewal. *Genes Dev.* **24**, 312-326.

Nichols, J., Silva, J., Roode, M. and Smith, A. (2009). Suppression of Erk signalling promotes ground state pluripotency in the mouse embryo. *Development* **136**, 3215-3222.

Ohnishi, Y., Huber, W., Tsumura, A., Kang, M., Xenopoulos, P., Kurimoto, K., Oleś, A. K., Araúzo-Bravo, M. J., Saitou, M., Hadjantonakis, A.-K. et al. (2014). Cell-to-cell expression variability followed by signal reinforcement progressively segregates early mouse lineages. *Nat. Cell Biol.* **16**, 27-37.

Oishi, Y., Manabe, I., Tobe, K., Ohsugi, M., Kubota, T., Fujiu, K., Maemura, K., Kubota, N., Kadowaki, T. and Nagai, R. (2008). SUMOylation of Krüppel-like transcription factor 5 acts as a molecular switch in transcriptional programs of lipid metabolism involving PPAR-delta. *Nat. Med.* **14**, 656-666.

Plusa, B., Piliszek, A., Frankenberg, S., Artus, J. and Hadjantonakis, A.-K. (2008). Distinct sequential cell behaviours direct primitive endoderm formation in the mouse blastocyst. *Development* **135**, 3081-3091.

Rossant, J. and Tam, P. P. L. (2009). Blastocyst lineage formation, early embryonic asymmetries and axis patterning in the mouse. *Development* **136**, 701-713.

Saiz, N., Williams, K. M., Seshan, V. E. and Hadjantonakis, A.-K. (2016). Asynchronous fate decisions by single cells collectively ensure consistent lineage composition in the mouse blastocyst. *Nat. Commun.* **7**, 13463.

Schrode, N., Saiz, N., Di Talia, S. and Hadjantonakis, A.-K. (2014). GATA6 levels modulate primitive endoderm cell fate choice and timing in the mouse blastocyst. *Dev. Cell* **29**, 454-467.

Singh, A. M., Hamazaki, T., Hankowski, K. E. and Terada, N. (2007). A heterogeneous expression pattern for Nanog in embryonic stem cells. *Stem Cells* **25**, 2534-2542.

Smith, A. (2017). Formative pluripotency: the executive phase in a developmental continuum. *Development* **144**, 365-373.

Takahashi, K. and Yamanaka, S. (2006). Induction of pluripotent stem cells from mouse embryonic and adult fibroblast cultures by defined factors. *Cell* **126**, 663-676.

Theunissen, T. W., Powell, B. E., Wang, H., Mitalipova, M., Faddah, D. A., Reddy, J., Fan, Z. P., Maetzel, D., Ganz, K., Shi, L. et al. (2014). Systematic identification of defined conditions for induction and maintenance of naive human pluripotency. *Stem Cell* **15**, 1-17.

Wicklow, E., Blij, S., Frum, T., Hirate, Y., Lang, R. A., Sasaki, H. and Ralston, A. (2014). HIPPO pathway members restrict SOX2 to the inner cell mass where it promotes ICM fates in the mouse blastocyst. *PLoS Genet.* **10**, e1004618.

Yamanaka, Y., Lanner, F. and Rossant, J. (2010). FGF signal-dependent segregation of primitive endoderm and epiblast in the mouse blastocyst. *Development* **137**, 715-724.

Yeo, J.-C., Jiang, J., Tan, Z.-Y., Yim, G.-R., Ng, J.-H., Göke, J., Kraus, P., Liang, H., Gonzales, K. A. U., Chong, H.-C. et al. (2014). Klf2 is an essential factor that sustains ground state pluripotency. *Cell Stem Cell* **14**, 864-872.

Ying, Q.-L., Wray, J., Nichols, J., Batlle-Morera, L., Doble, B., Woodgett, J., Cohen, P. and Smith, A. (2008). The ground state of embryonic stem cell self-renewal. *Nature* **453**, 519-523.

Supplemental Figures

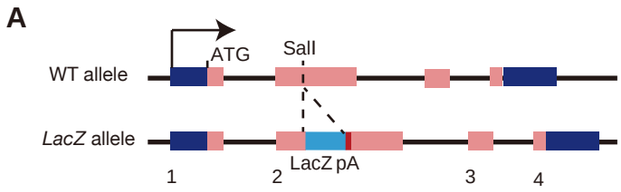

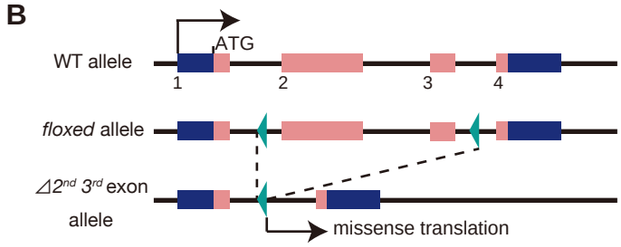

C

	+/+	+/Δ2nd3rd exon	Δ2nd3rd exon/Δ2nd3rd exon	empty decidua
E3.5	14	25	15	
E6.5	7	19	0	2

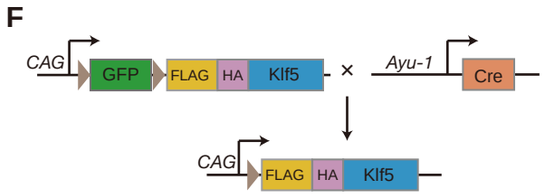

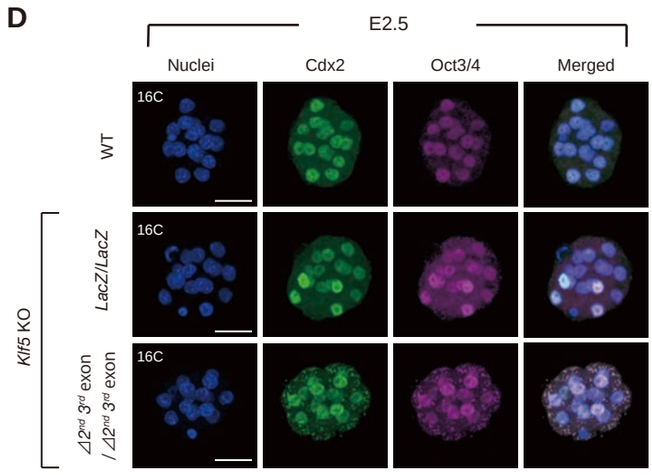

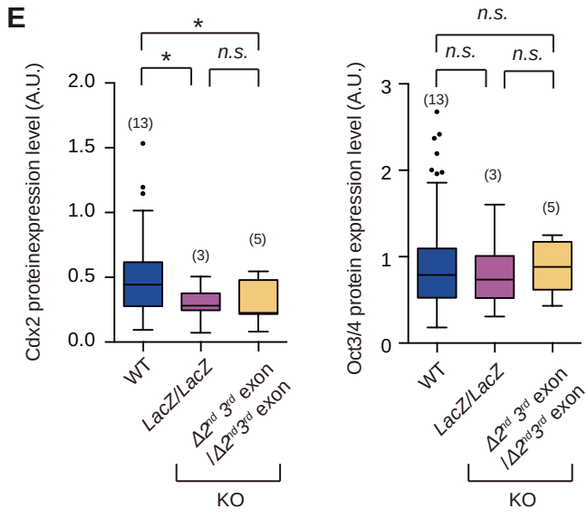

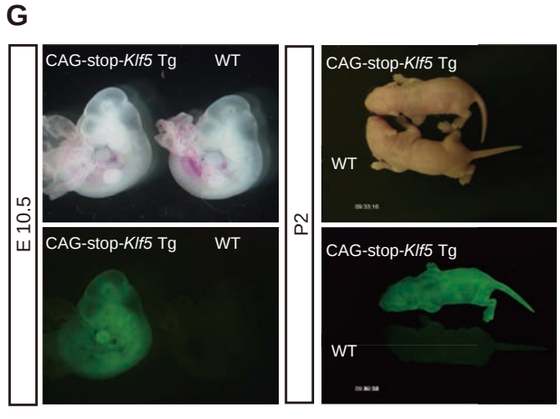

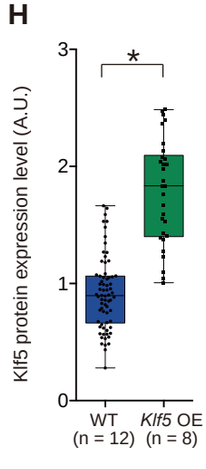

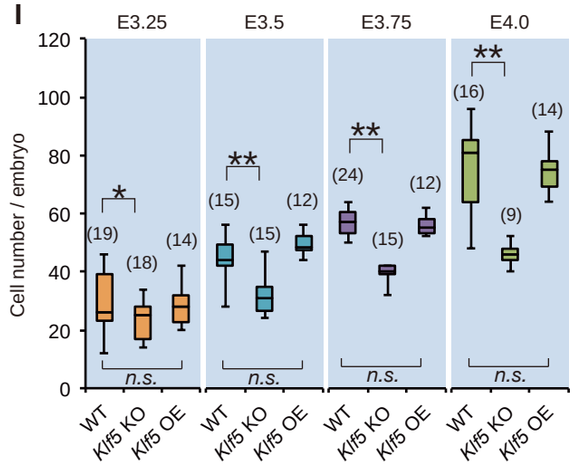

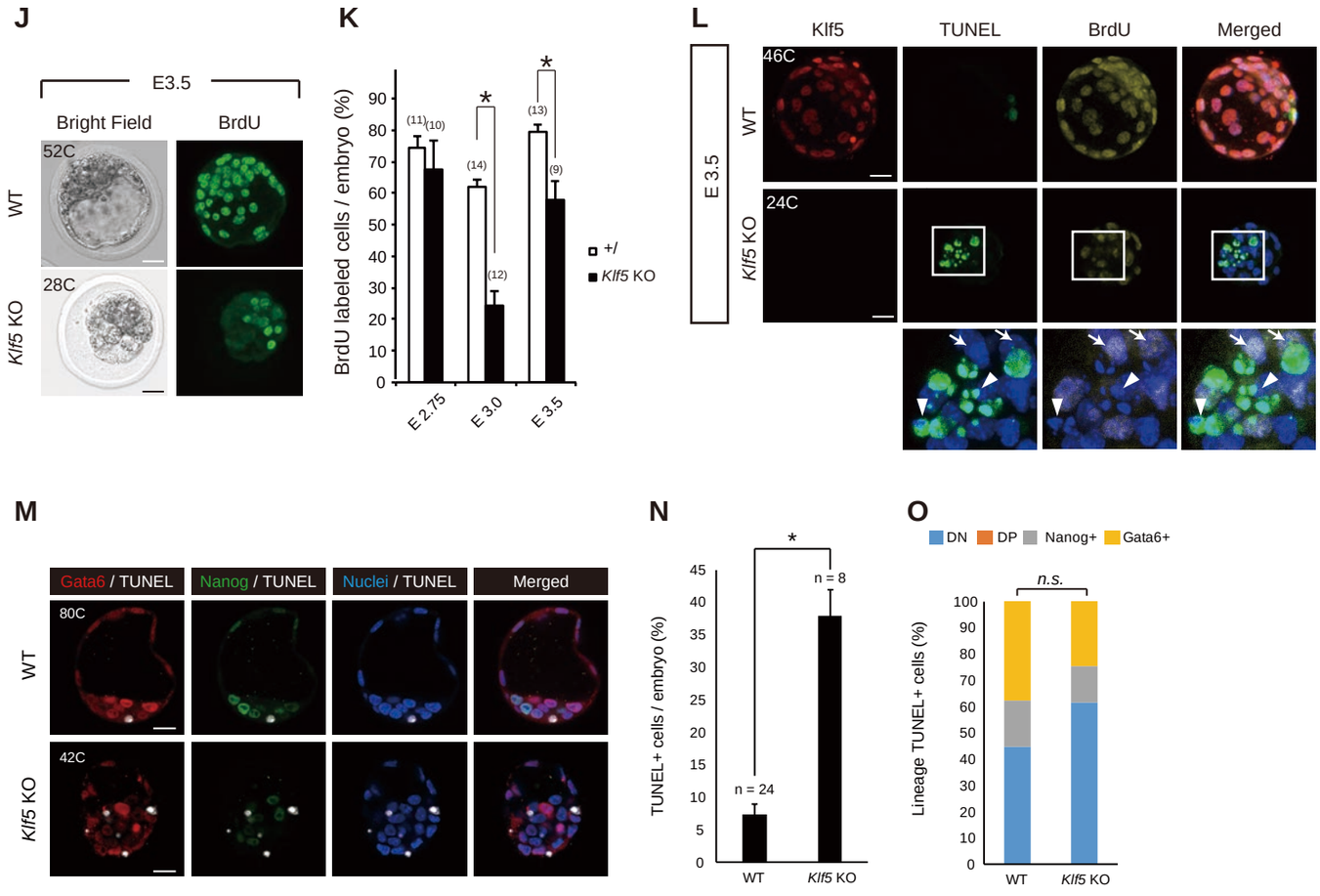

Figure S1: The *Klf5* mutant alleles and *Klf5* conditional activation mice used for this study. *LacZ* knock-in allele for *Klf5*. SalI is a restriction enzyme site and pA is the polyadenylation signal sequence. (B) Conditional knockout allele for *Klf5*. Two loxP sites were introduced that flanked exons 2 and 3. Exons 2 and 3 were removed by expressing Cre transiently to generate a null allele that lacked functional Klf5. ATG is the initiation codon. (C) Genotype of embryos from newly generated *Klf5*Δ2nd3rd exon heterozygous mouse intercrosses at the preimplantation (E3.5) and postimplantation (E6.5) stages. (D) Expression of Oct3/4 and Cdx2 in WT, *Klf5LacZ/LacZ*, and *Klf5*Δ2nd3rd exon/*Klf5*Δ2nd3rd exon embryos at E2.5. C, cell number. Scale bars represent 25 µm. (E) Tukey box plots showing Cdx2 and Oct3/4 protein levels at E2.5. Embryo numbers are shown in brackets. Asterisks indicate statistical significance: *P < 0.01; n.s., not significant; Mann–Whitney U-test. (F) Generation of conditional *Klf5* OE mice. The CMV early enhancer/chicken beta actin (CAG) promoter was used to drive GFP, and FLAG/HA-tagged Klf5 after Cre excision, in the transgene (Tg). (G) GFP expression in conditional *Klf5* OE mice during embryonic and postnatal stages. (H) Tukey box plots showing Klf5 protein levels at E3.5 blastocysts. Asterisks indicate statistical significance: *P < 0.01; Mann–Whitney U-test. (I) Tukey box plots of the numbers of cells per embryo. Embryo numbers are shown in brackets. Asterisks indicate statistical significance: *P < 0.01; ** P < 0.001; n.s., not significant; Mann–Whitney U-test. (J, K) BrdU incorporation in WT and *Klf5* KO blastocysts at E3.5. Percentage of BrdU incorporated cells in WT and *Klf5* KO blastocysts is shown in (K). Embryo numbers are shown in brackets. Asterisks indicate statistical significance: *P < 0.01; Mann–Whitney U-test. C, cell number. Scale bars represent 20 µm. (L) *Klf5* KO embryos showed increased apoptosis by TUNEL assays at the blastocyst stages. Note that the cells not incorporating BrdU from E3.25 to E3.5 tended to undergo apoptosis. Arrow indicates BrdU+ cells. Arrowhead indicates TUNEL+ cells that does not incorporate BrdU. C, cell number. Scale bars represent 20 µm. (M) TUNEL+ cells in WT and *Klf5* KO embryos at E3.75. Representative confocal optical section images showing colocalization of TUNEL+ cells with Gata6+ and Nanog+ cells. C, cell number. Scale bars represent 20 µm. (N) Percentages of TUNEL+ cells in WT and *Klf5* KO embryos at E3.75. Asterisks indicate statistical significance: *P < 0.01; Mann–Whitney U-test. (O) Localization of TUNEL+ cells in Nanog+, Gata6+, Nanog/Gata6 double-positive (DP), and double-negative (DN) cells in WT and *Klf5* KO embryos at E3.75. Distributions of TUNEL+ cells are shown as percentages of total cell numbers. There was no significant difference in the distribution of TUNEL+ cells between WT and *Klf5* KO embryos. Fisher's exact test was used for statistical analysis. n.s., not significant.

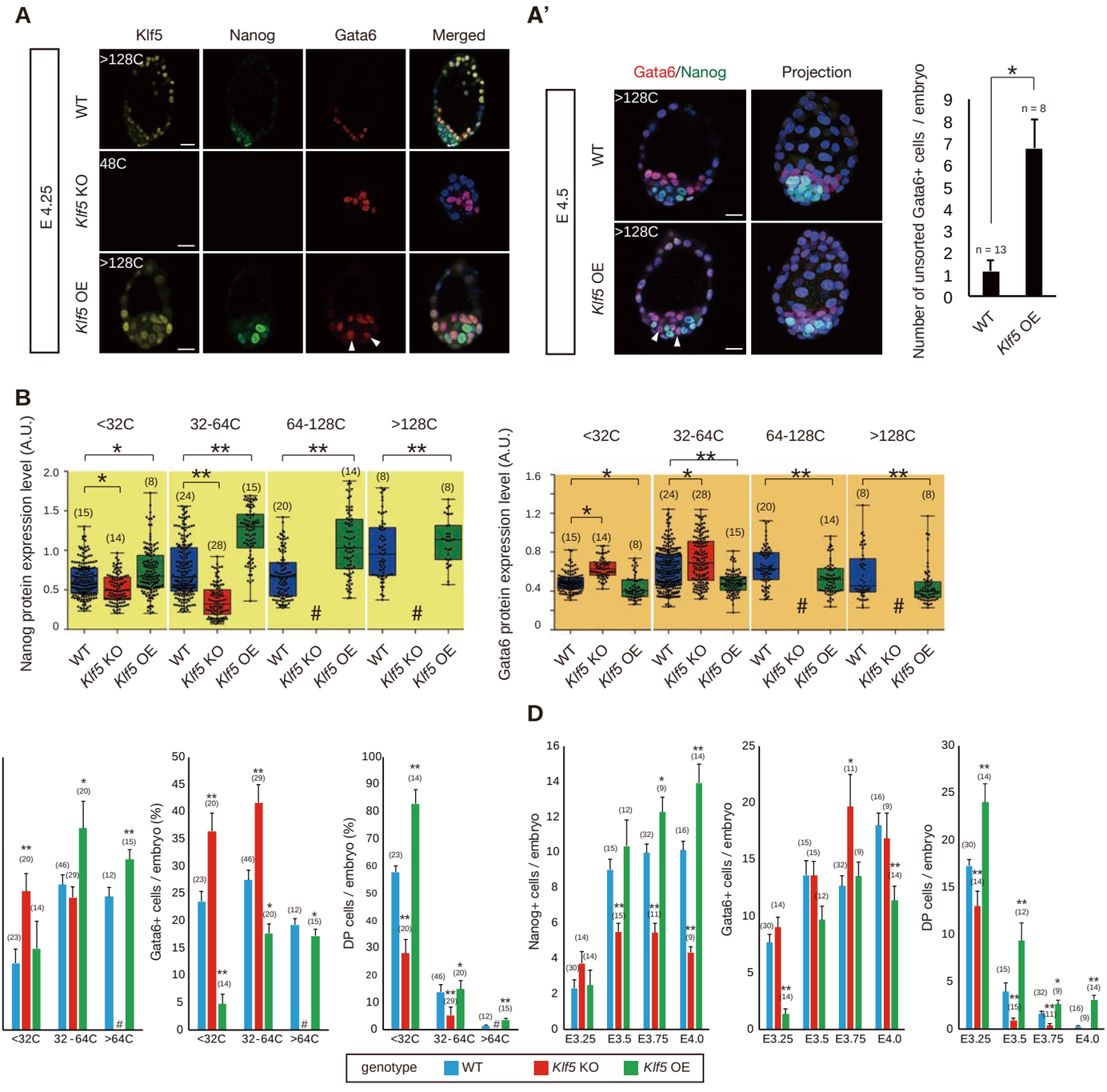

Figure S2: Skewed EPI and PrE lineage specification in *Klf5* KO and *Klf5* OE blastocysts. (A) Expressions of Nanog and Gata6 in WT, *Klf5* KO and *Klf5* OE embryos at E4.25. Images are confocal microscopy cross-sections. C, cell number. Scale bars represent 20 µm. (A′) Expressions of Nanog and Gata6 in WT and *Klf5* OE embryos from E4.5. Arrowheads indicate the unsorted Gata6+ cells located interiorly. Note that number of the unsorted Gata6+ cells is significantly increased in *Klf5* OE embryos at E4.5. Scale bar represent 20 µm. (B) Tukey box plots of Nanog and Gata6 protein expression levels. Embryo numbers are shown in brackets. A.U., arbitrary unit. # indicates no embryo obtained. (C) Percentages of Nanog+, Gata6+ and DP cells per embryo. # indicates no embryo obtained. (D) Absolute numbers of Nanog+, Gata6+ , and DP cells per embryo. Asterisks in (A'), (B) and (C) indicate statistical significance compared with WT: *P < 0.01; ** P < 0.001; Mann–Whitney U-test.

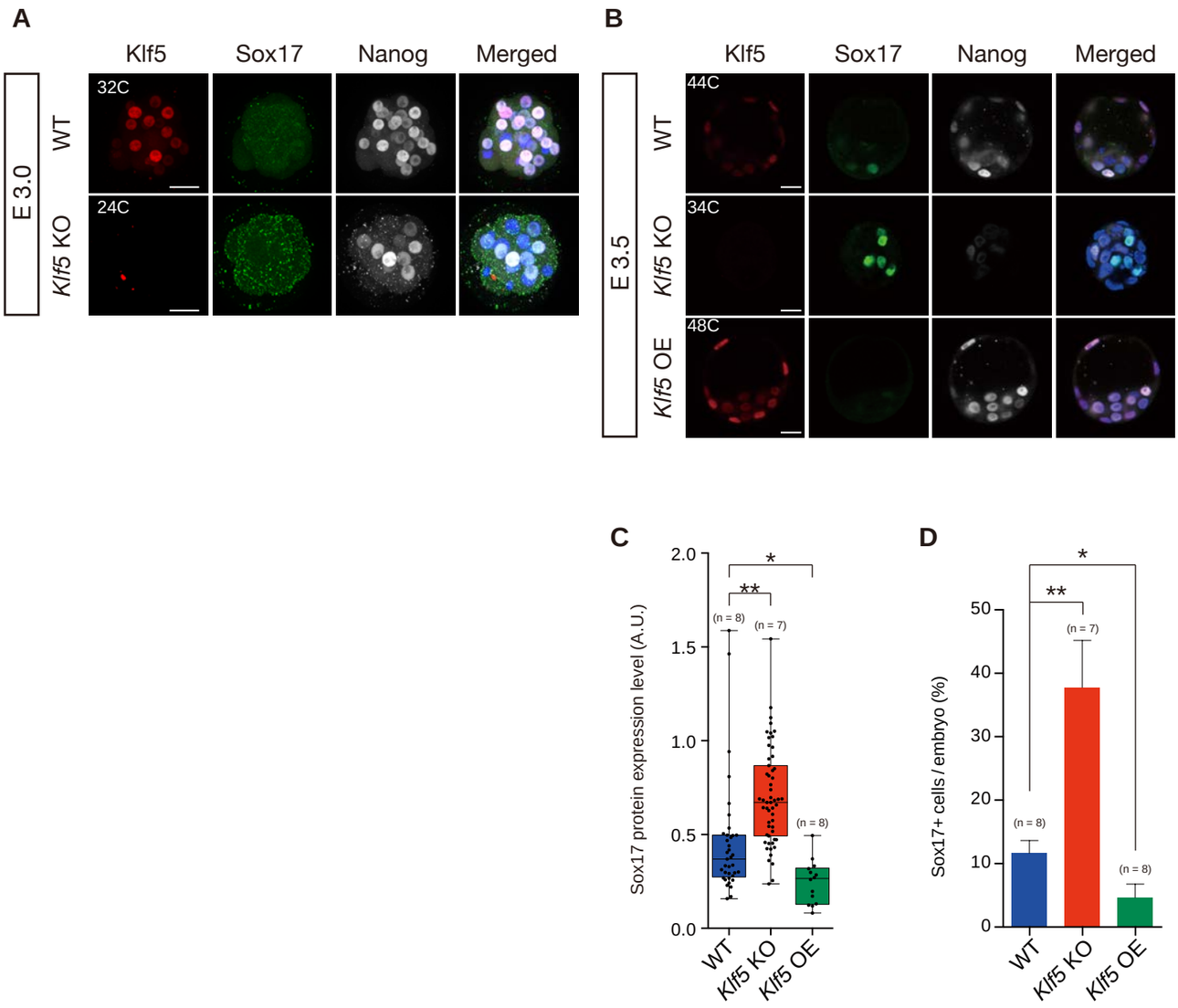

Figure S3: Accelerated PrE lineage specification in *Klf5* KO blastocysts. (A) Expressions of Sox17 and Nanog in WT and *Klf5* KO embryos at E3.0. Sox17 protein was not detected in the nuclear of both WT and *Klf5* KO embryos at this stage. Images are projection images from confocal microscopy. C, cell number. Scale bars represent 20 µm. (B) Expressions of Sox17 and Nanog in WT, *Klf5* KO and *Klf5* OE embryos at E3.5. Note that Sox17 protein expression levels are dramatically upregulated and downregulated in *Klf5* KO embryos and *Klf5* OE embryos, respectively. Images are confocal microscopy cross-sections. C, cell number. Scale bars represent 20 µm. (C) Tukey box plots of the levels of Sox17 expression in cells at E3.5. A.U., arbitrary unit. Embryo numbers are shown in brackets. (D) Percentage of Sox17+ cells per embryo at E3.5. Asterisks in (C) and (D) indicate statistical significance: *P < 0.01; ** P < 0.001; Mann–Whitney U-test.

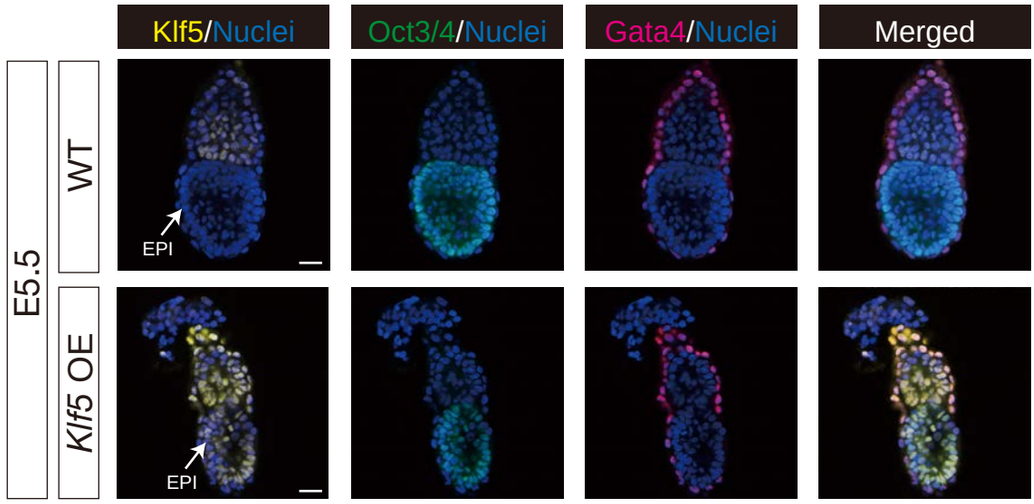

Figure S4: Overall normal development of *Klf5* OE embryos. Oct3/4 and Gata4 expressions in WT or *Klf5* OE embryos at E5.5. Arrows indicate postimplantation EPI. Scale bars represent 20 μm.

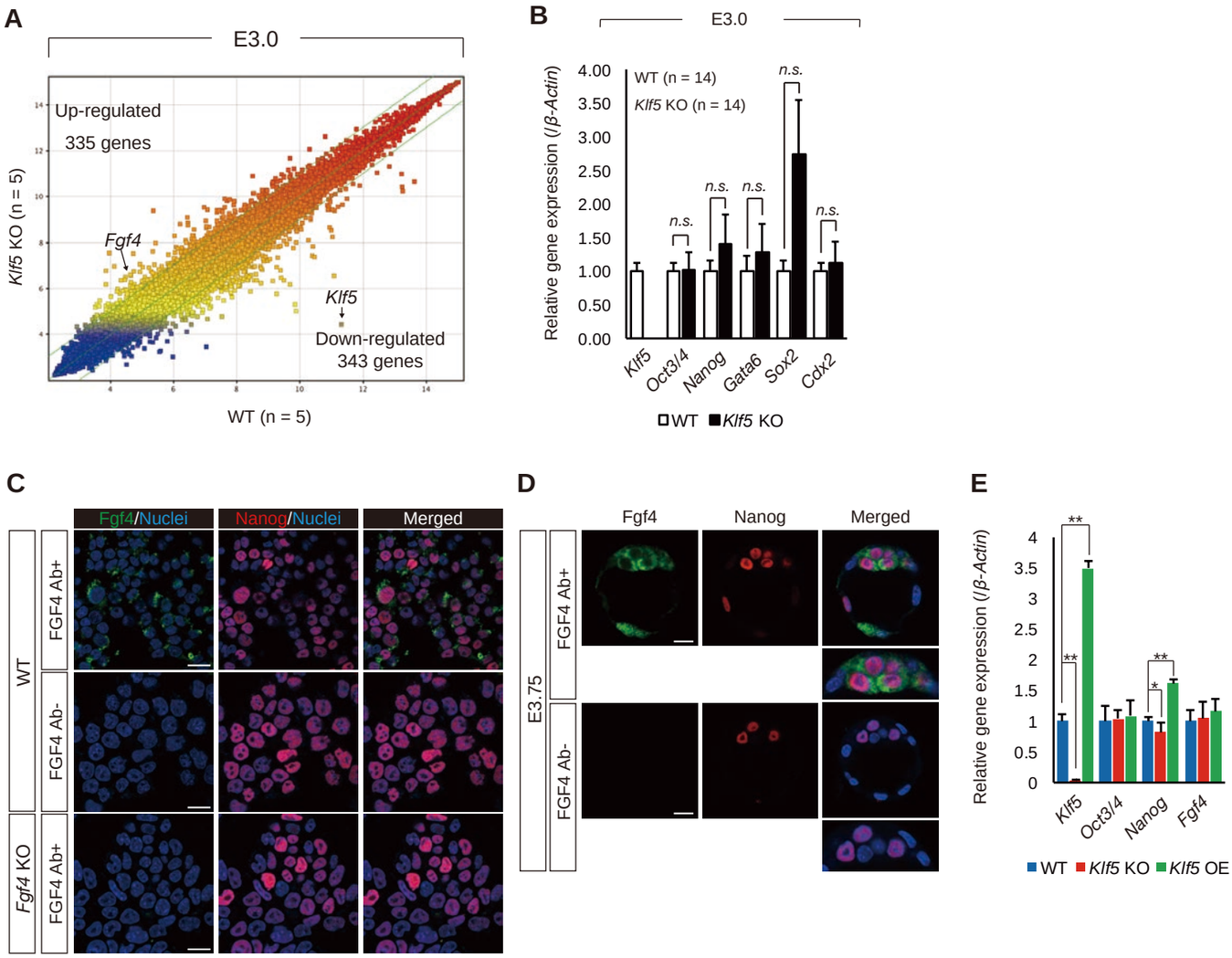

Figure S5: *Fgf4* expression and validation of anti-FGF4 antibody. (A) A scatter plot of genes upregulated/downregulated in *Klf5* KO embryos compared with WT embryos at E3.0. n; number of samples analysed. (B) Expression of embryonic transcription factors in *Klf5* KO blastocysts. n.s, not significant. (C) Validation of anti-FGF4 antibody with *Fgf4* KO ES cells. Note that the anti-FGF4 antibody recognises FGF4 in mouse ES cells. Scale bars represent 20 µm. (D) Detection of FGF4 expression in epiblast cells of WT embryos at E3.75 with the anti-FGF4 antibody. Scale bars represent 20 µm. (E) *Fgf4* mRNA expression in *Klf5* KO and *Klf5* OE ES cells. Asterisks indicate statistical significance: *P < 0.01; ** P < 0.001; Mann–Whitney U-test.

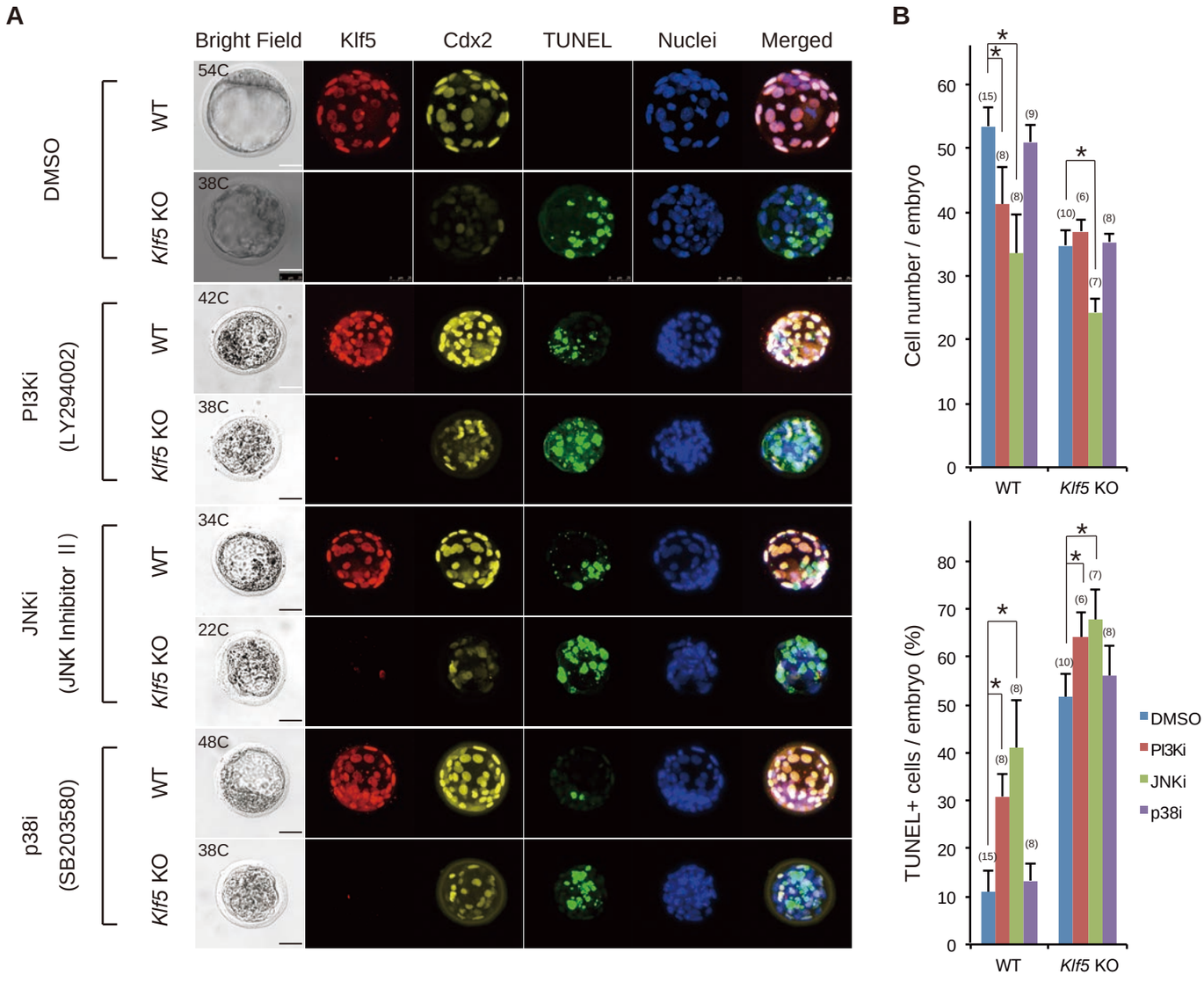

Figure S6: Ability of chemical inhibitors (i) against JNK, p38, and PI3K to rescue the phenotype of *Klf5* KO blastocysts. (A) Expression of Klf5 and Cdx2 and TUNEL+ cells in WT and *Klf5* KO blastocysts at E3.75. Embryos at E2.75 were collected and cultured in the presence of inhibitors of PI3K (LY294002, 10 µM), JNK (JNK inhibitor II, 5 µM), and p38 (SB203580, 10 µM) for 24 h. C, cell number. Scale bars represent 25 µm. (B) The upper panel shows the number of cells per embryo and the lower panel shows percentages of TUNEL+ cells per embryo. Embryo numbers are shown in brackets. Asterisks indicate statistical significance: *P < 0.01; Mann–Whitney U-test.

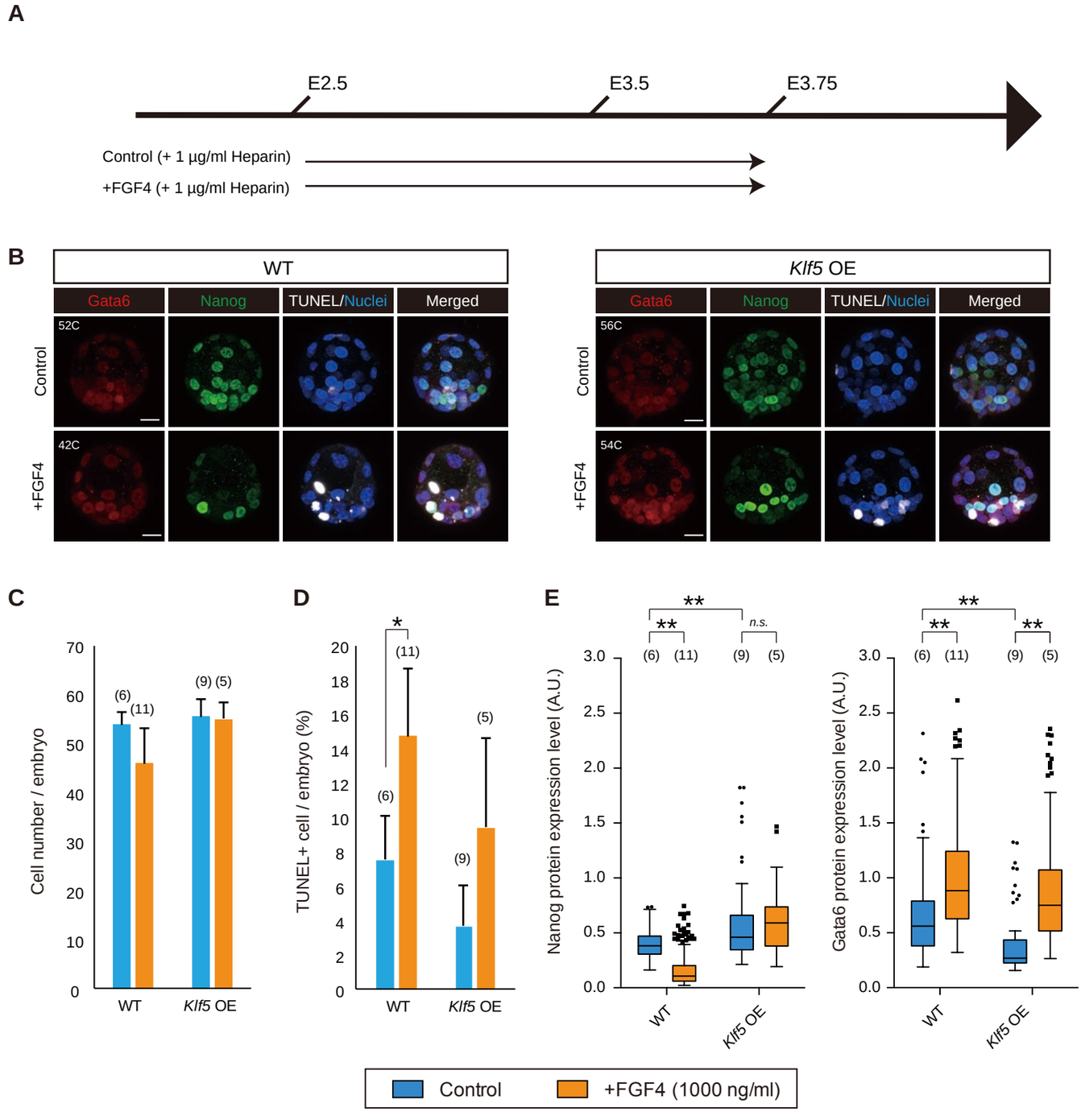

Figure S7: Stimulation of FGF–ERK signalling by FGF4 in *Klf5* OE embryos. (A) Outline of experiment to assess the effect of Fgf–ERK pathway stimulation by exogenous FGF4. WT and *Klf5* OE embryos were collected at E2.5 and cultured in the presence of FGF4 (1000 ng/ml) and heparin (1 µg/ml) until E3.75. (B) Effects of FGF4 on lineage specification and apoptosis induction in *Klf5* OE embryos at E3.75. Images are projection images from confocal microscopy. Scale bars represent 20 µm. (C) Average cell numbers in FGF4 treated WT and *Klf5* OE embryos. Embryo numbers are shown in brackets. (D) Percentages of TUNEL+ cells in WT and *Klf5* OE embryos cultured in the presence of FGF4. Embryo numbers are shown in brackets. (E) Turkey box plots of Nanog and Gata6 protein expression levels. Embryo numbers are shown in brackets. A.U., arbitrary unit. Asterisks in (C), (D) and (E) indicate statistical significance: *P < 0.05; **P < 0.01; Mann–Whitney U-test. n.s., not significant.

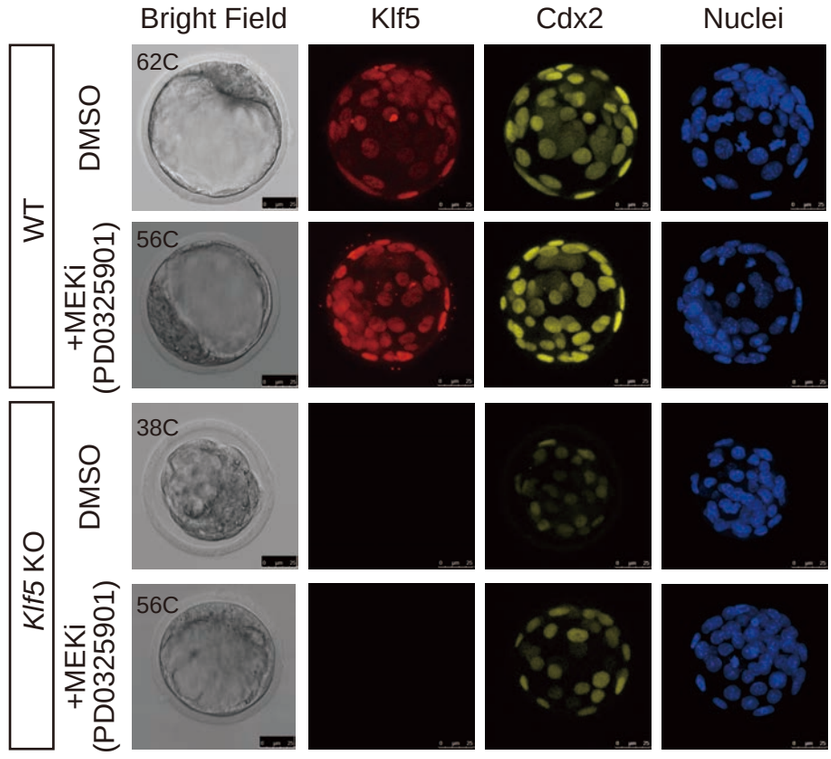

Figure S8: Inhibition of ERK signalling does not rescue the reduced Cdx2 expression of *Klf5* KO blastocysts. The reduced Cdx2 expression in *Klf5* KO embryos was not rescued by treatment with a MEK inhibitor (MEKi). Dimethyl sulfoxide was the solvent control. C, cell number. Scale bars represent 25 μm.

Table S1: List of genotyping primers sequences

Name	Primer Sequence (Forward)	Primer Sequence (Reverse)	Usage
Klf5_WT allele	CCTGTTACCATTTTCAGCCACCAGA	TGAAGATATTGTTCACCTCCTGTGGT	for *Klf5* KO embryos
Klf5_deletion allele	AGGCCTGATAAAATAACCTAGTCCA	TAAGCACCGGTGCCTAACATGGTA	for *Klf5* KO embryos
Klf5_2-4ex	GTACACCATGCCAAGTCAGTTTCTTC	GTTGGCACACCATGCACTGGAAC	for *Klf5* OE embryos
Cre	GGACATGTTCAGGGATCGCCAGGCGT	GCATAACCAGTGAAACAGCATTGCTG	for *Klf5* OE embryos

Table S2: List of antibodies

Primary Antibody	Supplier	Catalogue Number	Dilution
mouse anti-Cdx2	BioGenex	MU392A-UC	1:300
rabbit anti-Nanog	Cosmobio	RCAB0001P	1:300
mouse anti-Oct3/4	SantaCruz	sc-5279	1:300
goat anti-Gata6	R&D	AF1700	1:300
goat anti-Gata4	SantaCruz	sc-1237	1:300
goat anti-Fgf4	R&D	BAF235	1:100
rat anti-Pdgfra	eBioscience	13-1401-82	1:300
goat anti-Sox17	R&D	AF1924	1:300
rat anti-Klf5	Kyowa KIRIN	a gift from Dr. Nagai	1:300
mouse anti-FLAG-M2	Sigma-Aldrich	F3165	4 μg
normal mouse IgG	SantaCruz	sc-2025	4 μg

Secondary Antibody	Supplier	Catalogue Number	Dilution
Cy3-conjugated donkey anti-mouse IgG	Jackson Immunoresearch	715-166-151	1:500
Cy3-conjugated donkey anti-rabbit IgG	Jackson Immunoresearch	711-165-152	1:500
Cy5-conjugated donkey anti-rat IgG	Jackson Immunoresearch	712-175-153	1:500
Alexa488-conjugated donkey anti-rabbit IgG	Molecular Probes	A21206	1:500
Alexa488-conjugated donkey anti-goat IgG	Molecular Probes	A110055	1:500
Alexa633-conjugated donkey anti-goat IgG	Molecular Probes	A21082	1:500
HRP-conjugated donkey anti-goat IgG	Jackson Immunologicals	705-035-147	1:500

Table S3: List of qPCR primers sequences

Primers for RT-qPCR

Gene	Primer Sequence (Forward)	Primer Sequence (Reverse)
Fgfr1	CCTCAGGAAACAGAAAACGATCT	CCCTCTAAGGCTTGAGTGGTGT
Fgfr2	ACAGCACCAGGAACCTACTTACACT	CTGTCCACTTATCAGGAAACAGTCT
Fgf4	AAGGCACCTGCCCTGTTCTG	GGGAGCTAGCTGGCTGAAGAAA
Gata6	ACTGAAGTAAGAAGAGATGGGCTTT	ATCTCTCAATCTTCCTTAGCAGACA
Pdgfra	CTAGCAGGTGACGCTTTGGA	GGCCAATCTGGCTCAGTCTT
Sox17	CAGTATCTGCCCTTTGTGTATAAGC	GTAGTTGCAATAGTAGACCGCTGAG
Oct3/4	TATTGAGTATTCCCAACGAGAAGAG	CTCAGGAAAAGGGACTGAGTAGAGT
Nanog	CTTTCACCTATTAAGGTGCTTGC	TGGCATCGGTTCATCATGGTAC
Sox2	CATGAGAGCAAGTACTGGCAAG	CCAACGATATCAACCTGCATGG
Cdx2	CACTTTAGTCGATACATCACCATCA	CTGCTTCTTCTTGATTTTCCTCTC
Klf5	CGATTCACAACCCAAATTTACC	GTATGAGTCCTCAGGTGAGCTTTTA
β-actin	CTGAGCGCAAGTACTCTGTGTG	GTGTAAAACGCAGCTCAGTAACAGT

Primers for ChIP-qPCR

Gene	Primer Sequence (Forward)	Primer Sequence (Reverse)
Fgf4_1	TGGGTCCTCACTCCTACCTG	AAGACAGGGAGCAGCACAGT
Fgf4_2	GTGTCACAGCAGCTCCAAGA	GAGGGATCAGCCTAGCAGTG
Fgf4_4_2	TCCTTAGGTGCTGGGAATTG	TGCCTGAAGCAACATAGCTG
Vegfr2	CCCTGTTCACAAGTAAATACACCTC	GTTGTATATTCAGCTCCTCACGAAT

Supplementary Materials and Methods.

Pluripotent stem cells. *Fgf4*$^{+/-}$ (clone 342) and *Fgf4*$^{-/-}$ (clone FD6) ES cells (kind gifts from Dr. Angie Rizzino (Wilder et al., 1997)) were cultured in DMEM + 10% Serum/LIF condition onto fibronectin-coated glass bottom dishes and were subjected to immunohistochemistry using an anti-FGF4 antibody.

Generation of *Klf5* KO mice and overexpressing transgenic mice. To generate a conditional allele for *Klf5*, a targeting vector was created in which two loxP sequences flanking exons 2 and 3 were introduced, and the vector was introduced into E14 ES cells. ES cells that had undergone homologous recombination were selected and used to prepare chimeric animals (details are available upon request). Then, the *Klf5* conditional KO mice were crossed with FLPe deleter mice to remove the PGK-neo cassette and further crossed with Cre deleter mice to obtain the $\Delta 2^{nd}3^{rd}$ exon allele that allows removal of almost the entire open reading frame. All experiments were performed in accordance with the Declaration of Helsinki and were approved by the Ethics Committee for Animal Experiments of Shiga University of Medical Science.

Conditional *Klf5*-overexpressing mice were generated as follows. A Venus-pA cassette followed by FLAG-HA tagged mouse Klf5 cDNA was inserted into a CAG vector and electroporated into C57B6/J ES cells. An ES cell line (clone N6) expressed a similar level of FLAG-HA tagged Klf5 protein as endogenous Klf5 after Cre excision. This clone was used to create chimeric animals for germ line transmission. Conditional *Klf5*-overexpressing mice were crossed with Ayu1-Cre, a germ line deletion mouse strain to overexpress FLAG-HA-tagged Klf5.

Immunohistochemistry with anti-FGF4 antibody. To obtain a clear FGF4 signal from preimplantation embryos, FGF4 staining was performed as previously described (Shimokawa et al., 2011) with modification. Briefly, embryos were fixed in 4% PFA for 15 min and then permeabilised in 30 μg/ml Proteinase K prepared in 0.1% Tween 20/PBS for 3 min at room temperature. For the blocking reaction, embryos were incubated in BlockingOne (Nacalai Tesque) for 30 min at room temperature. Embryos were incubated with goat anti-FGF4 antibody in the blocking reagent at 4 °C overnight. After the embryos were washed with 0.1% Tween 20/PBS, they were incubated with HRP-conjugated donkey anti-goat IgG antibody (Jackson ImmunoResearch) for 3 h at room temperature. An Alexa 488 Tyramide SuperBoost Kit (Thermo) was used to detect the FGF4 protein according to the manufacturer's protocol.

Confocal microscopy analysis and image data acquisition.

For discrimination of inner and outer cells at E3.25, the distance of WT embryo nuclei (Cdx2+ TE nuclei and Cdx2- inner cell nuclei) to the nearest-neighbouring surface was measured using ImageJ. A threshold distance to distinguish Cdx2+ TE nuclei from Cdx2- inner cell nuclei was set. Subsequently, this threshold was used to manually discriminate inner and outer cells in DIC images of the embryos.

After confocal imaging, the embryos were washed in PBS and placed individually into polymerase chain reaction (PCR) tubes. To extract genomic DNA, 10 μl of 500 μg ml^{-1} proteinase K (Nacalai Tesque) was added to each PCR tube and incubated at 56 °C for 45 min in a thermal cycler. After the proteinase K had been inactivated at 95 °C for 10 min. Aliquots (3 μl) of the extracted DNA were used as templates for PCR. PCR was performed with KOD FX Neo (TOYOBO) according to the manufacturer's recommendation and primers described in Table S1.

Chromatin immunoprecipitation (ChIP) assays. The ChIP assays were performed as described (Ito et al., 2013). Cells were cultured in 10-cm plates to approximately 80% confluence, and one plate was used for each immunoprecipitation run. The cells were fixed with 1% formaldehyde for 10 min at room temperature with swirling. Glycine was added to a final concentration of 0.125 M, and the incubation was continued for an additional 5 min at room temperature. The cells were washed twice with ice-cold PBS, harvested by scraping, pelleted, and resuspended in sodium dodecyl sulphate (SDS) lysis buffer (50 mM Tris-HCl, pH 8.1, 1% SDS, 10 mM EDTA, and protease inhibitors from Nacalai Tesque). The samples were sonicated four times for 15 min each with an interval of 30 sec using a UH-50 sonicator (SMT, Tokyo, Japan). The samples were then centrifuged at 13,200 rpm at 4 °C for 15 min. After an aliquot (whole-cell extract) had been removed as an input sample, the supernatants were diluted 10-fold in ChIP dilution buffer (16.7 mM Tris-HCl, pH 8.1, 16.7 mM NaCl, 1.2 mM EDTA, 1.1% Triton X-100, 0.01% SDS). The diluted samples were pre-cleared with 50 μl of protein G Sepharose beads (GE Healthcare) for 2 h at 4 °C with rotation, and then the supernatants were incubated at 4 °C overnight with 4 μg of normal mouse IgG (Santa Cruz Biochemicals) and anti-FLAG-M2 antibody (Sigma-Aldrich). The immunocomplexes were collected by incubation with 100 μl of protein G Sepharose beads (GE Healthcare) for 1 h at 4 °C with rotation. The beads were washed with the following buffers: low salt wash buffer (0.1% SDS, 1% Triton X-100, 2 mM EDTA, 150 mM NaCl, and 20 mM Tris–HCl; pH 8.1), high salt wash buffer (0.1% SDS, 1% Triton X-100, 2 mM EDTA, 500 mM NaCl, and 20 mM Tris–HCl; pH 8.1), and LiCl wash buffer (0.25 mM LiCl, 1% IGEPAL-C630, 1% sodium deoxycholate, 1 mM EDTA, and 10 mM Tris–HCl; pH 8.1). Finally, the beads were washed twice with 1 ml of TE buffer (1 mM EDTA and 10 mM Tris–HCl; pH 8.0). The immunocomplexes were then eluted by adding 200 μl of elution buffer (10 mM DTT, 1%

SDS, 100 mM $NaHCO_3$). The eluate was collected and the cross-linking was reversed by adding NaCl to a final concentration of 200 mM and incubating for 6 h at 65 °C. The remaining proteins were digested by adding proteinase K. The DNA was precipitated with phenol, precipitated with ethanol, and quantified by qPCR. The sequences of the primers used for ChIP-qPCR are listed in Table S2.

ChIP-sequencing (ChIP seq) data analysis. ChIPseq data FASTQ files were downloaded from the EMBL-EBI site [E-GEOD-49848; Klf5, Aksoy *et al*. (Aksoy et al., 2014)]. ChIPseq reads were mapped to the mouse reference genome (mm9) using the Burrows–Wheeler Aligner software. Uniquely mapped reads were used for peak calling by CCAT3 version 3.0. Peak regions were filtered for false discovery rate values ≤ 0.05. We produced a RefSeq gene that had a Klf5 binding site within 20 kb by determining the overlap between the ChIPseq peak regions and RefSeq genes extended by 20 kb both up- and downstream. To visualise the ChIPseq tag counts in the UCSC Genome Browser, mapped reads were extended and converted into the bedGraph format by using the genomecov function of BEDTools.

References

Aksoy, I., Giudice, V., Delahaye, E., Wianny, F., Aubry, M., Mure, M., Chen, J., Jauch, R., Bogu, G. K., Nolden, T., et al. (2014). Klf4 and Klf5 differentially inhibit mesoderm and endoderm differentiation in embryonic stem cells. *Nat. Commun.* **5**, 3719.

Ito, I., Waku, T., Aoki, M., Abe, R., Nagai, Y., Watanabe, T., Nakajima, Y., Ohkido, I., Yokoyama, K., Miyachi, H., et al. (2013). A nonclassical vitamin D receptor pathway suppresses renal fibrosis. *J. Clin. Invest.* **123**, 4579–94.

Shimokawa, K., Kimura-Yoshida, C., Nagai, N., Mukai, K., Matsubara, K., Watanabe, H., Matsuda, Y., Mochida, K. and Matsuo, I. (2011). Cell surface heparan sulfate chains regulate local reception of FGF signaling in the mouse embryo. *Dev. Cell* **21**, 257–72.

Wilder, P. J., Kelly, D., Brigman, K., Peterson, C. L., Nowling, T., Gao, Q. S., McComb, R. D., Capecchi, M. R. and Rizzino, A. (1997). Inactivation of the FGF-4 gene in embryonic stem cells alters the growth and/or the survival of their early differentiated progeny. *Dev. Biol.* **192**, 614–29.